nature communications 10-4-2022

BK channels of five different subunit combinations underlie the *de novo* KCNMA1 G375R channelopathy

Yanyan Geng[1], Ping Li[2,4], Alice Butler[2] Bill Wang[2], Lawrence Salkoff[2,3,5], and Karl L. Magleby[1,5,*]

[1]Department of Physiology and Biophysics, University of Miami Miller School of Medicine, Miami FL 33136, USA; [2]Department of Neuroscience and [3]Department of Genetics, Washington University St. Louis, MO 63110, USA. [4]Present address: Department of OBGYN, Washington University St. Louis, MO 63110, USA. [5]These authors contributed equally.

[*]Corresponding Author: Karl L. Magleby, Department of Physiology and Biophysics, University of Miami Miller School of Medicine, Miami FL 33136
Email: kmagleby@miami.edu

Abstract

The molecular basis of a severe developmental and neurological disorder associated with a *de novo* G375R variant of the tetrameric BK channel is unknown. Here we address this question by recording from single BK channels expressed for a heterozygous G375R mutation. Five different types of functional BK channels were observed: 3% were WT, 12% were homomeric mutant, and 85% were three different types of hybrid channels. All channel types except WT showed a marked gain-of-function in voltage activation and a smaller loss-of-function in single channel conductance, with both becoming more pronounced as the number of mutant subunits per tetrameric channel increased. The molecular phenotype suggested codominance for the two homomeric channels and partial dominance for the hybrid channels. A model in which BK channels are randomly assembled from mutant and WT subunits, with each subunit contributing increments of activation and conductance, approximated the molecular phenotype of the heterozygous G375R mutation.

Introduction

The BK channel (Slo1, KCa1.1) is a large conductance K^+ selective channel that is synergistically activated by Ca^{2+} and voltage[1-16]. BK channels are homotetrameric proteins comprised of four large pore-forming (alpha) subunits >1200 amino acids[15] (Supplementary Fig. 1) encoded by the *KCNMA1* gene. BK channels are widely expressed in many cell types where they modulate smooth muscle contraction[17], transmitter release[18], circadian rhythms[19], repetitive firing[20,21], and cellular excitability[22]. Mutations in the *KCNMA1* gene that encode the (alpha) subunit of BK channels are associated with a wide range of disease, including epilepsy, dyskinesis, autism, multiple congenital abnormalities, developmental delay, intellectual disability, axial hypotonia, ataxia, cerebral and cerebellar atrophy, bone thickening, and tortuosity of arteries[23-28].

Studies of the pathogenic properties of BK channels associated with disease have often been incomplete, focusing on the homomeric mutant channels. Yet, for a mutation heterozygous with the wild-type (WT) allele, mutant and WT subunits have the potential to assemble into five different stoichiometries for tetrameric channels with likely differences in functional properties (Fig. 1)[29-33].

Here we show that this is the case for a *de novo* G375R mutation in the (alpha) subunit of BK channels associated with the Liang-Wang Syndrome[25]. Three unrelated children who carried this mutation had a syndromic neurodevelopmental disorder associated with severe developmental delay and polymalformation syndrome[25]. The G375R mutation, located on the back side of the S6 pore-lining helix of the alpha subunit (Supplementary Fig. 1), replaces the hydrogen side chain of glycine with a large arginine side chain that might be expected to distort the subunit structure and gating[34] as well as add a positive charge that may alter conductance.

To assess the functional effects of a G375R mutation, we recorded currents from whole cells and excised macro patches of membrane after injecting a 1:1 mixture of G375R mutant and WT cRNA encoding for mutant and WT subunits into *Xenopus* oocytes, to mimic a *de novo* mutation heterozygous with respect to the WT allele. When compared to WT, the currents from the 1:1 injection were left shifted more than -120 mV. This large negative shift in activation indicated a pronounced gain-of-function (GOF) mutation at the cellular level, providing a possible explanation for the severity of the disease associated with the heterozygous G375R mutation.

To investigate the molecular basis underlying the cellular response, detailed single-channel recording[35] after the 1:1 injection suggested that five different types of functional BK channels were expressed: 3% were WT, 12% were homomeric mutant, and 85% were three different types of hybrid (heteromeric) channels. All channel types except WT showed a marked GOF in voltage activation and a smaller LOF in single channel conductance, with both becoming more pronounced as the number of mutant subunits per channel increased. Codominance was observed for the two homotetrameric channels, with homomeric WT channels active at the most positive voltage range of channel activity and homomeric mutant channels active at the most negative. Partial dominance was observed for the three types of hybrid channels, which were activated at voltages intermediate between those of WT and homomeric mutant channels. A model in which BK channels were randomly assembled from mutant and WT subunits, with each subunit

contributing increments of activation and conductance, could approximate the molecular phenotype of the heterozygous G375R BK mutation. The possibility that a channelopathy patient with a heterozygous BK channel mutation synthesizes five different types of BK channels in their neurons and other cells, four with aberrant properties, presents a daunting challenge for treatment.

Results

G375R subunits left shift BK channel activation. To examine what effect a *de novo* G375R mutation of the pore forming subunit of BK channels would have on channel function when co-expressed with WT subunits, we first compared macroscopic currents flowing through large numbers of WT BK channels expressed following injection of WT cRNA into *Xenopus* oocytes, to those currents expressed following injection of a 1:1 mixture of mutant and WT cRNA to mimic a heterozygous mutation. Injection of a blank without cRNA served as a control. Voltages were stepped from a holding potential of -80 mV to more negative and more positive voltages to reveal the voltage dependent activation of the expressed currents (Fig. 2A; Supplementary Fig. 2). Voltage steps to +50 mV were required to appreciably activate WT BK currents generated from the injection of WT cRNA. In contrast, following a 1:1 injection of G375R mutant and WT cRNA, the expressed BK channels currents were hyperactive, being already active at -140 mV, with depolarization further increasing the response (Fig. 2B, Supplementary Fig. 2). The aberrant BK channels from the 1:1 injection that are responsible for these hyperactive currents could be either homomeric mutant channels, hybrid channels, or both (Fig. 1).

The negative shift in activation for currents expressed from the 1:1 injection was so pronounced that large numbers of aberrant BK channels would have been open at voltages near the resting membrane potential of -60 mV. If aberrant currents expressed similarly in neurons, the flux of K^+ through opened BK channels would act to drive the membrane potential towards the equilibrium potential for K^+, opposing depolarization of the cell and facilitating repolarization, which could interfere with normal neuronal function. Thus, at the level of whole cell and macro patch recording, the heterozygous G375R mutation gave a pronounced gain-of-function (GOF) phenotype because much less depolarization was required to activate BK currents. Some of the disease phenotypes associated with this mutation might be due to such GOF behavior. In contrast, Liang et al. reported a LOF for G375R because they observed no BK currents for homomeric mutant channels[25]. Their conclusion of a LOF vs. our conclusion of a GOF will be considered in detail in a later section.

To quantify the average negative voltage shift in activation for the BK currents following injection of a 1:1 mixture of G375R and WT cRNA, when compared to WT currents following injection of only WT cRNA, we recorded currents from macro patches of membrane which were excised from oocytes after channel expression. This allowed the composition of the solution at the inner membrane surface to be controlled, which was not the case for the whole cell

113 recordings in Fig. 2. For a solution at the intracellular membrane surface containing <0.01 μM
114 Ca^{2+} (~0 Ca^{2+}), WT BK currents did not activate appreciably until the membrane potential
115 exceeded 100 mV (black circles), whereas BK currents from the 1:1 injection of G375R mutant
116 and WT cRNAs started to activate at very negative voltages of -80 mV (Fig. 3B). The mean
117 voltage for half activation (V_h) was 182 ± 5.4 mV (n = 6) for WT BK currents and 61.5 ± 16 mV
118 (n = 12) for BK currents from the 1:1 injection, giving a mean left shift of -120 mV in voltage
119 activation for the currents following a 1:1 injection when compared to WT ($p < 0.0001$). This left
120 shift in voltage activation was even greater in the presence of 300 μM Ca^{2+} (Supplementary Fig.
121 3). The 1:1 injection also decreased the voltage sensitivity of activation compared to WT, with a
122 slope of 38.5 ± 1.8 (n = 8) mV per e-fold change compared to 23.2 ± 1.36 mV (n = 6) for WT
123 currents ($p < 0.0001$).
124 The large negative shifts in voltage activation observed for whole cell recordings following a
125 1:1 injection of mutant and WT cRNA (Fig. 2; Supplementary Fig. 2) are thus also observed for
126 macro patch recordings under conditions in which the intracellular solution and Ca^{2+} are
127 controlled (Fig. 3; Supplementary Fig. 3).
128 Whole cell and macro patch recordings are useful to show the average response of many
129 hundreds to thousands of BK channels, but they provide limited information about the properties
130 of the underlying channels, unless all channels are identical, which is unlikely to be the case for a
131 heterozygous mutation, as shown in Fig. 1. To investigate the channels underlying the negative
132 shifts in BK currents in Figs. 2 and 3 for a 1:1 injection of mutant and WT cRNA to mimic a
133 mutation heterozygous with the WT allele, we first consider the possible channel types and
134 frequencies of expression that might be expected for a heterozygous mutation. We then record
135 from individual channels expressed following a 1:1 injection of mutant and WT cRNA to see if
136 the expectations are met.
137
138 **BK channels of five different potential stoichiometries and six different subunit arrangements**
139 **could theoretically be expressed for a mutation heterozygous with WT.** WT and mutant
140 subunits arising from a heterozygous mutation could potentially assemble into tetrameric BK
141 channels with five different stoichiometries and six different subunit arrangements, each with
142 potentially different properties (Fig. 1)[29-33]. If it is assumed that there is equal production of
143 mutant and WT subunits, that subunits assemble randomly to form tetrameric channels, and that
144 each assembled channel has the same probability of reaching the surface membrane, then the
145 channels expressed for a heterozygous mutation would consist of 6% WT channels, 25%
146 comprised of 1 mutant and 3 WT subunits, 38% comprised of 2 mutant and 2 WT subunits, 25%
147 comprised of 3 mutant and 1 WT subunit, and 6% homomeric mutant channels (Fig. 1). On this
148 basis, 94%, of the expressed channels could be pathogenic, comprised of 88% hybrid
149 (heteromeric) channels of mixed subunits and 6% homomeric mutant channels, with only 6%
150 WT channels (Fig. 1).
151

152 **Assembled channels.** The term assembled channels will be used to refer to those BK channels
153 that are assembled and expressed following injection of a 1:1 mixture of G375R mutant and WT
154 cRNA into *Xenopus* oocytes, to mimic a heterozygous mutation. Assembled channels could
155 theoretically include five types of channels with different stoichiometries and six types of
156 channels if subunit arrangement is considered (Fig. 1). An individual assembled channel could
157 then be any one of the six channel types. It is the combined activity of the six potential types of
158 assembled channels that would determine the BK currents for a heterozygous mutation.
159
160 **Assembled channels display an abnormally wide range of V_h.** To explore if multiple channel
161 types contribute to the negative shift in V_h resulting from a G375R BK subunit mutation
162 heterozygous with WT (Figs. 2, 3, Supplementary Figs. 2, 3), we used the unique ability of the
163 patch clamp technique[31,35-37] to isolate and record from individual assembled channels expressed
164 following a 1:1 injection of mutant and WT cRNA into *Xenopus* oocytes. For each of the 33
165 individual assembled channels studied, single-channel currents were recorded over a range of
166 voltages (Fig. 4*A*) to obtain plots of open probability (Po) vs. voltage (Fig. 4*B*, red curves). The
167 Po-V plots for the 33 individual assembled channels had a voltage for half activation (V_h) that
168 ranged from -152 mV to +151 mV, for a span of 303 mV (Fig. 4*B*, red Po-V curves). This very
169 wide range in V_h supports the idea that there are multiple types of assembled channels with
170 different properties arising from different subunit composition (Fig. 1).
171
172 **Assembled channels include WT, homomeric mutant, and hybrid channels.** To identify the
173 types of BK channels expressed following a 1:1 injection of mutant and WT cRNA, the Po-V
174 curves of the 33 individual assembled channels in Fig. 4B were compared to Po-V curves
175 obtained from individual WT and homomeric mutant channels. The WT and homomeric mutant
176 channels were obtained by single channel recording after injection of only WT cRNA or only
177 mutant cRNA, respectively. The WT channels had V_h values that spanned a narrow range from
178 +140 to +176 mV (Fig. 4C, black Po-V curves), and the homomeric mutant channels had V_h
179 values that ranged from -272 mV to -38 mV (Fig. 4C, blue Po-V curves). The homomeric mutant
180 channels had a surprisingly wide range of V_h for channels of presumed identical composition of
181 four mutant subunits, but all were in a far more negative voltage range than WT channels. The
182 reason for such a wide voltage range in V_h for the homomeric mutant channels is not known, but
183 perhaps channels with four mutant subunits can assume different conformations with markedly
184 different activation properties, depending on mutant side-chain orientation (Supplementary Fig.
185 1).
186 To facilitate the identification of the types of assembled channels, the Po-V curves of the
187 individual 33 assembled channels from Fig. 4B were overlaid on plots of the V_h ranges of the Po-
188 V curves for known WT (gray shading) and homomeric mutant (blue shading) channel controls
189 in Fig. 4D. One of the 33 assembled channels had a Po-V curve that overlapped with the known
190 WT channel controls (Fig. 4D), suggesting that this assembled channel was WT with four WT

subunits. Four of the 33 assembled channels had Po-V curves that overlapped with the known homomeric mutant channel controls (Fig. 4D), suggesting that these four assembled channels were homomeric mutant, comprised of four mutant subunits. The remaining 28 assembled channels had Po-V curves that did not overlap with the known WT or homomeric mutant channel controls (Figs. 4D), but fell in between, suggesting that these 28 assembled channels were all hybrid channels comprised of a mix of mutant and WT subunits, because hybrid channels were the only types of channels remaining (Fig. 1). In this study, assembled channels with V_h values in the ranges of WT, hybrid, and homomeric mutant channels will be referred to as WT, hybrid, and homomeric mutant channels, respectively, with the understanding that these classifications are based on V_h values.

For the sampled group of 33 assembled channels, ~3% (1/33) were WT, ~85% (28/33) were hybrid, and ~12% (4/33) were homomeric mutant (Fig. 4B-D). Fig. 1 predicts ~6% WT, ~88% hybrid, and ~6% homomeric mutant channels. Thus, for the G375R mutation heterozygous with WT, both experimental and theoretical considerations suggest that most (85-88%) of the expressed assembled channels will be hybrid, with much smaller fractions of homomeric mutant and WT channels. All hybrid and homomeric mutant channels displayed negative shifts in activation compared to WT, with the greatest negative shifts for the homomeric mutant channels. Consequently, both theoretical and experimental considerations suggest that 94-97% of the BK channels arising from a G375R mutation heterozygous with WT would display aberrant negative shifts in activation, even though only 50% of the subunits synthesized in a cell would be mutant.

Three functional types of hybrid assembled channels. Assembled channels were found to be comprised of 85% hybrid channels, 3% WT, and 12% homomeric mutant (Fig. 4). The 85% hybrid channels themselves could consist of three types, with one, two, or three mutant subunits per channel replacing an equal number of WT subunits (Fig. 1). To explore this possibility, a histogram of the V_h values of the 33 assembled channels from Fig. 4B was plotted in Fig. 5A as red bars. Histograms of known WT channel controls (black bars) and homomeric mutant channel controls (blue bars) from Fig. 4C are also plotted. The subunit compositions of the homomeric mutant and WT channel controls are known and placed above these two types of channels in Fig. 5A. As expected from Fig. 4D, four of the assembled channels had V_h values that overlapped with those of homomeric mutant channels, suggesting that they were homomeric mutant channels; one assembled channel overlapped with WT, suggesting that it was a WT channel; and the remaining 28 assembled channels had V_h values falling in between those of homomeric mutant and WT channels, identifying them as hybrid channels (Fig. 1).

The V_h values of the 28 hybrid channels fell into three apparent clusters with mean values of about 1.4, 59 and 96 mV (Fig. 5A). Three clusters of V_h for hybrid channels would be expected from Fig. 1 if each mutant subunit replacing a WT subunit added an increment of negative shift in V_h, as suggested by Fig. 4 and in Fig. 6 in a later section. Accordingly, as a working hypothesis, the different subunit combinations for hybrid channels from Fig. 1 have been placed

above the three clusters of hybrid channels in Fig. 5A to obtain a stepwise negative shift in V_h for each additional mutant subunit replacing a WT subunit. Because only three clusters of hybrid channels were observed, instead of four, it has been assumed that the hybrid channels with two mutant and two WT subunits, but of different subunit arrangement, contribute to the same cluster. Fig. 5A then suggests five different types of functional assembled channels: homomeric mutant, three types of hybrid channels, and WT channels, as indicated. The percentages of expression of the five functional types of assembled channels were then calculated from Fig. 5A and presented in Fig. 5B. Simulation of 1 million groups of 33 assembled channels, assuming equal production of mutant and WT subunits followed by random assembly into tetrameric channels, indicated that the experimentally observed percentages in Fig. 5B were not significantly different from the predictions of Fig. 1 (Supplementary Fig. 4).

Whereas the observation of three apparent clusters of V_h values for the hybrid assembled channels (Fig. 5) is consistent with theoretical predictions (Fig. 1), peaks can occur by chance alone in histograms of binned data of limited sample size[38]. Consequently, additional experiments would be needed to determine whether V_h values for hybrid channels can consistently be resolved into three peaks, but an observation of such distinct peaks is not required for support of Fig. 1, as variability in V_h among channels of the same type[39] might be sufficient to obscure distinct peaks.

Linear Incremental model for the contributions of mutant and WT subunits to V_h. WT BK channels comprised of four WT subunits had a mean V_h of about 160 mV, and homomeric mutant BK channels comprised of four mutant subunits had a mean V_h of about -80 mV (Figs. 4A, C; Fig. 5A). As all four subunits contribute to the gating of BK channels[4,5,31], these observations suggest that each WT subunit contributes an increment of positive shift to V_h and each mutant subunit contributes an increment of negative shift. In support of this hypothesis, a linear incremental model in which each WT subunit in a channel added +40.5 mV to V_h and each mutant subunit added -16.7 mV, provided an approximate description of the observed V_h's for the five types of assembled channels (Fig. 5C dashed line; model in figure legend). The net effect of replacing a WT subunit with a mutant subunit was a -57.2 mV shift in V_h to account for the loss of the positive shift contributed by the removed WT subunit and the addition of the negative shift contributed by the added mutant subunit.

Dual action of G375R subunits on V_h and single channel conductance *g*. In addition to the negative shift in activation induced by replacing WT subunits with G375R mutant subunits (Figs. 2-5), replacing WT subunits with mutant subunits also decreased single-channel conductance (Fig. 6A, B). The mean single-channel conductance of WT channels was 312 ± 4 pS. This decreased to 245 ± 6 pS for hybrid channels, and further decreased to 190 ± 14 pS for homomeric mutant channels. These decreases were significant (Fig. 6 legend). Hence, single-channel conductance decreased as mutant subunits replaced WT subunits. The decreased single-

269 channel conductance may arise from the larger volume and positive charge of the mutant
270 arginine side chains replacing the single hydrogen atom of the glycine side chains on the four S6
271 segments lining the conductance pathway of the BK channel (Supplementary Fig. 1). The added
272 volume of the sidechains could decrease the volume of the inner vestibule and the added positive
273 charge may act to repel K^+ from the inner cavity. Both actions can reduce single channel
274 conductance in BK channels[40-42].
275 To examine the relationship between single-channel conductance and V_h, the single-channel
276 conductance for each channel was plotted against V_h for the same channel in Fig. 6C for the
277 indicated channel types. A linear relationship was observed (Fig. 6C; R = 0.86, P < 0.0001).
278 When taken together, the data in Figs. 6B and 6C are consistent with the idea that replacing a
279 WT subunit with a mutant subunit adds both an increment of negative voltage shift to V_h and a
280 step decrease in single-channel conductance. Thus, at the single-channel level, the heterozygous
281 G375R mutation acts simultaneously as a GOF mutation to shift voltage activation to more
282 negative voltages (Figs. 4, 5), and as a loss-of-function (LOF) mutation to decrease single-
283 channel conductance (Fig. 6). At the whole cell and macro patch level, the increase in currents
284 from the GOF negative shift in activation would dominate the LOF reduction in single-channel
285 conductance, producing large left shifted currents (Figs. 2, 3; Supplementary Figs. 2 and 3). The
286 LOF in conductance would act to decrease the consequences of the negative shift in activation.
287
288 **Linear Incremental model for the contributions of mutant and WT subunits to single-channel**
289 **conductance.** A linear incremental model in which each WT subunit contributes 76.5 pS to
290 single channel conductance and each mutant subunit contributes 46.1 pS could approximate the
291 single channel conductance for the five types of assembled channels (Fig. 6D dashed line; model
292 in figure legend).
293
294 **WT, hybrid, and G375R homomeric mutant channels are expressed in the HEK293 cell**
295 **expression system.** Liang et al.[25] reported that no potassium currents were recorded from
296 excised macro patches following transfection of HEK293T cells with plasmids coding for
297 G375R mutant BK subunits. In contrast, we found that functional single homomeric mutant
298 channels were readily expressed following injection of *Xenopus* oocytes with cRNA coding for
299 mutant BK G375R subunits (Fig. 4A, C). To examine if these differences in channel expression
300 were due to differences in expression systems, we transfected HEK293 cells with WT cDNA to
301 generate WT channels, with mutant G375R cDNA to generate homomeric mutant channels, and
302 with a 1:1 mixture of WT and mutant cDNA to mimic the generation of channels that would
303 normally arise from a heterozygous mutation. We found that the transfected HEK293 cells
304 displayed robust whole-cell BK currents for each of the three different types of transfection (Fig.
305 7A). The G-V plots for transfection with WT cDNA or 1:1 transfection with WT and mutant
306 cDNA were very similar to those we obtained using the *Xenopus* oocyte expression system
307 (compare Fig. 7 with Fig. 3). We also found that whole cell G375R homomeric mutant currents

308 from HEK293 cells had V_h values within the broad range of V_h values of single-channel
309 recordings from patches of membrane excised from *Xenopus* oocytes (Fig. 4).
310 Hence, in both *Xenopus* oocytes and HEK293 expression systems we observed functional
311 G375R homomeric mutant currents that displayed a marked negative shift in activation
312 consistent with a GOF mutation. This contrasts with the observations of Liang et al.[25] who did
313 not observe potassium currents for G375R transfection of HEK293T cells. They reported G375R
314 as a LOF mutation. The reason for the difference in observations is not known, but we found that
315 the viability of *Xenopus* oocytes injected with G375R cRNA was reduced (see Methods).
316
317 **Whole cell and macro-patch currents can obscure mechanism.** The narrow error bars for the
318 macro currents recorded from whole oocytes and excised macro patches (Figs. 2 and 3;
319 Supplemental Figs. 2 and 3) following injection of WT cRNA or a 1:1 injection of mutant and
320 WT cRNA, indicated that the mean responses recorded from hundreds to thousands of channels
321 were repeatable. Narrow error bars for mean responses do not necessarily indicate that the
322 individual channels underlying the mean response have near identical properties, as this was not
323 the case for the macro currents following 1:1 injections of mutant and WT cRNA, where
324 individual assembled channels for 1:1 injections had a very wide range of V_h that spanned over
325 300 mV (Fig. 4B). In spite of this wide range for individual channels, the mean G-V data
326 following the 1:1 injections were reasonably well described by a single Boltzmann function (Fig.
327 3B, blue line through red diamonds), but were better described (red line) by assuming five
328 underlying channel types (Fig. 1) as described in the legend to Fig. 3.
329
330 **Discussion**
331 The heterozygous G375R BK channel variant has been associated with a devastating human
332 phenotype that includes malformation syndrome and severe neurological and developmental
333 disorders[25]. This variant has only appeared in the human population when heterozygous with
334 WT, perhaps because a homozygous G375R variant may not permit viability because of the
335 extreme GOF phenotype we observed for homomeric mutant channels. To gain insight into the
336 pathogenicity of this variant, currents from whole cells, macro patches, and single channels were
337 recorded from BK channels expressed following a 1:1 injection of G375R mutant and WT cRNA
338 to mimic a G375R mutation heterozygous with WT.
339 Recordings from whole cells and macro patches, both of which contain many hundreds to
340 thousands of channels, indicated that the voltage required for half activation, V_h, of the current
341 following a 1:1 injection, was left shifted to more negative potentials by about -120 mV
342 compared to WT currents (Figs. 2 and 3; Supplementary Figs. 2 and 3), indicating a pronounced
343 net GOF phenotype on channel activation. The aberrant BK channels underlying the negative
344 shifts in activation would lead to a much greater fraction of BK channels being open at negative
345 membrane potentials, including at potentials near the resting potential (Figs. 2, 3 and
346 Supplementary Figs. 2, 3), which would oppose cellular depolarization, altering cellular function.

To explore the underlying molecular basis for the aberrant current activation associated with the heterozygous G375R variant, we used high resolution single channel recording to isolate and characterize the BK channels, termed assembled channels, that are assembled and expressed following injection of a 1:1 mixture of G375R mutant and WT cRNA. Theoretical considerations based on equal production and random assembly of mutant and WT subunits suggest there could be multiple types of assembled channels with different subunit combinations[29,30,32,33] (Fig. 1) Consistent with this possibility, our analysis suggested that five different types of functional BK channels were expressed: 3% were WT, 12% were homomeric mutant, and 85% were three different types of hybrid channels of mixed subunits (Fig. 4, Fig. 5A, B). The frequencies of expression of these five types of functional assembled channels were not significantly different (Supplementary Fig. 4) from the theoretical predictions of Fig. 1 based on equal production and random assembly of subunits. This suggests that the processes involved in subunit production, assembly, and expression do not distinguish significantly between the mutant and WT alleles or subunits, so that phenotypic differences arise at the level of individual channels.

The three types of hybrid channels comprising 85% of the expressed assembled channels, had properties falling between those of mutant and WT channels, that varied with their apparent subunit composition (Figs. 4-6). Ninety-seven percent of the assembled channels, all except for the 3% WT, displayed both GOF negative shifts in activation and LOF decreases in single-channel conductance (Figs. 4-6). Hence, most of the expressed channels for the heterozygous G375R mutation displayed aberrant properties. The values of V_h and single channel conductance for each of the five types of functional assembled channels could be predicted with a linear incremental model in which each mutant and WT subunit in each of the five types of functional assembled channels acted relatively independently to contribute increments of both V_h and single-channel conductance to the molecular phenotype of the channel (Figs. 5C, 6D).

A potential mechanism to produce the five functional types of assembled channels for a heterozygous G375R BK channel mutation, then, is equal production and random assembly of mutant and WT subunits into channels of five different subunit compositions, where the V_h and single-channel conductance of each channel type are determined by independent contributions from each of the four subunits in a channel. Each WT subunit adds increments of 40.5 mV to V_h and 76.5 pS to single channel conductance, and each mutant subunit adds increments of -16.7 mV to V_h and 46.1 pS to single channel conductance.

To our knowledge, this is the first time that the types of functional channels expressed for a heterozygous mutation, their specific phenotypes, frequencies of expression, and contributions of individual subunits have been revealed in such molecular detail (Figs. 4-6). With this molecular information in hand, it is now possible to classify the heterozygous G375R mutation with regards to inheritance of genetic disease, and also the individual molecular phenotypes of the five types of expressed functional channels.

For classification with regard to genetic disease, we suggest that the heterozygous G375R mutation be labeled as an assembly-mediated dominant-positive mutation, following the

386 terminology of Backwell and Marsh[33]. Assembly-mediated to indicate that mutant and WT
387 subunits assemble into multiple types of functional channels for the tetrameric BK channel,
388 dominant because the inclusion of only a single copy of the mutant *KCNMA1* gene leads to
389 disease[25], and positive to indicate an aberrant GOF in the activation of BK currents (Figs. 2, 3,
390 7). The net result of this assembly-mediated dominant-positive mutation in the tetrameric BK
391 channels is that a disproportionate fraction (94-97%) of the expressed channels display aberrant
392 activation due to the random assembly of mutant and WT subunits into functional channels
393 (Figs. 1, 4, 5). A dominant-positive GOF phenotype has been described previously for the
394 heterozygous G88R mutation of the TASK-4 K^+ channel in the heart, based on a study using
395 whole cell currents[43].
396 A dominant-positive effect is an analogy[33] to the well-known dominant-negative effect
397 observed for some types of protein complexes and channelopathies[33,44-49] Both can cause
398 disease: dominant positive from a GOF and dominant-negative from complete or partial LOF,
399 and both have a disproportionate fraction of the channels affected.
400 Whereas an assembly-mediated dominant-positive classification of the heterozygous G375R
401 mutation is useful to suggest a basis of genetic disease at the level of whole cell and macro patch
402 currents through BK channels, it describes only part of the molecular phenotype. Consequently,
403 to characterize the molecular phenotype we suggest that random assembly of mutant and WT
404 subunits for the heterozygous G375R mutation produces five functional types of assembled
405 channels: WT, mutant, and three types of hybrid channels of mixed subunit composition. All
406 channel types except WT simultaneously display a GOF in activation and a partial LOF in
407 single-channel conductance.
408 The genetic dominance of the various channel types expressed for a heterozygous mutation is
409 mixed and complex. Codominance was observed for the WT and homomeric mutant channels
410 and partial dominance was observed for the three types of hybrid channels. Support for
411 codominance is that the mutant and WT channels expressed when mimicking a heterozygous
412 mutation had the same molecular phenotypes as homomeric mutant and WT channels expressed
413 after injection of only mutant or WT cRNA, respectively (Figs. 4 and 5). Support for partial
414 dominance is that the three types of hybrid channels had their own values of V_h and single
415 channel conductance that were distinct from each other and fell in the range between those of the
416 homomeric mutant and WT channels (Figs. 5C, 6D). The levels of partial dominance in the
417 linear incremental model (Figs. 5C and 6D) were determined by the numbers of mutant and WT
418 subunits per channel acting relatively independently of one another, rather than by mutant
419 subunits altering the function of WT subunits, as in some classical descriptions of dominant-
420 negative. It is remarkable that a single base pair substitution in one allele of a pair of alleles that
421 encode for the alpha subunit of BK channels would result in WT channels plus four aberrant
422 channel types, each with different molecular phenotypes that simultaneously display dominant
423 positive and dominant negative effects, with the five types of functional channels displaying
424 either co-dominance or one of three levels of partial dominance.

How do our observations of a relatively independent interactions of the G375R mutant and WT pore-forming subunits compare to interactions of these subunits with regulatory subunits? Wang et al.[50] found that single BK channels comprised of four subunits could be associated with from 0 to 4 regulatory β2-subunits per channel, with each β2-subunit giving incremental changes in V_h. Hence both mutated and WT pore forming subunits[36] (Fig. 5) and the non-pore forming regulatory β2-subunits[50] can give incremental changes in gating, but such incremental changes per subunit are not necessarily universal, so each type of subunit will need to be checked. A single BK channel comprised of four subunits can also include up to four regulatory γ1-subunits, but a single γ1-subunit per channel is sufficient to induce the full gating shift induced by γ1-subunits[51,52].

Devising therapies for the *de novo* G375R heterozygous mutation will be challenging. Theoretical and experimental observations (Figs. 1, 4, 5) suggest that most (94 to 97%) of the channels for a mutation heterozygous with WT would be pathogenic, with only 3 to 6% of the channels WT. The pathogenic channels would consist of multiple channel types, each with large differences in activation properties and smaller differences in conductance (Figs. 4 - 6). Therapies to block or inactivate the pathogenic channels would ideally silence the multiple types of pathogenic channels while leaving any WT channels intact. Even if such selective blockers could be devised, it is unlikely that the remaining 3 to 6% of WT channels would be sufficient to restore normal cellular function. Effective therapies will likely require replacing or silencing the mutant alleles, or preventing mutant subunits from assembling with themselves and WT subunits if/when such techniques become practical in humans.

Methods

Constructs. Experiments were performed using the human large conductance calcium-activated potassium (BK) channel (hSlo1) KCNMA1 transcript: GenBank: U23767.1[3] for WT, and a G375R mutation (VFFIL**G**GLAMF to VFF IL**R**GLAMF) was constructed to match the G375R *de novo* variant described by Liang et al.[25]. G375R is at the same position as G310 in Tao and MacKinnon[15], which they called the gating hinge residue. The numbering differs because Tao and MacKinnon[15] used an alternative transcript missing the first 65 amino acids compared to U23767.1. Both our hSlo1 WT cRNA plasmid and WT mammalian transfection plasmid contain the same hSlo1 insert and are described in McCobb et. al.[3]. Overlap extension PCR cloning was used to generate the G375R mutation, which was verified by sequencing. The new construct was linearized downstream of the end of coding and transcribed with T3 using Invitrogen's T3 mMessage mMachine kit to make cRNA for injection into *Xenopus* oocytes. To mimic the effects of a heterozygous mutation, G375R mutant and WT cRNA were mixed in a 1:1 ratio by weight before injection into oocytes. For expression in HEK293 cells, two mammalian transfection plasmids were created. DNA fragments containing the complete channel cDNAs of either the WT or G375R mutant and two unique restriction sites flanking it were amplified by PCR and ligated into mammalian transfection plasmids, which were verified by sequencing.

464
465 **Expression of BK channels in oocytes for whole cell recording.** Defolliculated *Xenopus* oocytes
466 were injected with 0.5-150 ng of cRNA using a Nanoject II (Drummond Scientific) and
467 incubated at 18 °C for 2-5 days before recording. Incubation was in ND96 complete medium
468 consisting of (mM) 96 NaCl, 2 KCl, 1.8 $CaCl_2$, 5 $MgCl_2$, and 5 HEPES adjusted to pH 7.5,
469 supplemented with 2.5 mM sodium pyruvate and 100 µg/ml each penicillin and streptomycin.
470 The two-microelectrode whole cell voltage-clamp recordings from oocytes were obtained in
471 ND96 medium with 1 mM added 4,4′-diisothiocyanatostilbene-2,2′-disulphonic acid disodium
472 salt hydrate (DIDS) to block the endogenous chloride conductance. Currents were obtained with
473 an Oocyte Clamp OC-725C amplifier (Warner Instrument Corp.) Recordings were low-pass
474 filtered at 1 kHz and digitized at 10 kHz. Electrodes were made with borosilicate glass capillaries
475 (World Precision Instruments) pulled with a Sutter Instrument Co. P-87 pipette puller and filled
476 with 3 M KCl.
477
478 **Macro patch and single-channel recordings from BK channels expressed in *Xenopus* oocytes.**
479 Oocytes were injected with 0.1-18 ng of cRNA and incubated at 18°C for 2-5 days in Barth's
480 Solution (mM): 88 NaCl, 1 KCl, 2.4 $NaHC0_3$, 0.33 $Ca(NO_3)_2$, 0.41 $CaCl_2$, 0.82 $MgSO_4$, 15 mM
481 HEPES, pH 7.6, plus 12 µM tetracycline. Macro and single channel currents were recorded from
482 inside-out patches of membrane[35] excised from oocytes at room temperature (21°C to 24°C).
483 pClamp 9.0 software (Molecular Devices) was used to drive an Axopatch 200B amplifier to
484 collect the currents. For macro patch current recordings, borosilicate pipettes with 0.5–2 MΩ
485 resistance were used. The macro currents were filtered at 10 KHz and sampled at 100 kHz. A
486 minus P/4 protocol was used to remove capacitive transients and leak currents. For single-
487 channel recordings, borosilicate pipettes with 8-12 MΩ resistance were used. The single-channel
488 currents were filtered at 5 KHz and sampled at 200 KHz. The pipette (external) solution
489 contained (mM): 160 KCl, 2 $MgCl_2$, 5 TES buffer, pH 7.0. The internal membrane surface of the
490 excised patches was perfused by two different solutions. The designated 0 Ca^{2+} solution had a
491 free Ca^{2+} <0.01 µM and contained (mM): 160 KCl, 1 EGTA, 1 HEDTA, and 10 HEPES, pH 7.0.
492 The solution with 300 µM internal Ca^{2+} contained (mM): 160 KCl, 0.3 $CaCl_2$, 10 HEPES, pH
493 7.0. Procedures to obtain oocytes from *Xenopus* laevis were approved by the University of
494 Miami Animal Care and Use Committee. Macro patch and single channel recordings were
495 analyzed with Clampfit 10.7 software (Molecular Devices) and SigmaPlot 12.
496 For injection of only G375R cRNA into *Xenopus* oocytes we found that it was difficult to get
497 giga-ohm seals of sufficient quality for macro patch recordings using the lower resistance
498 electrodes required for such recordings. Hence, macro patch currents are not presented for
499 injection of only G375R cRNA into oocytes. However, it was still possible to obtain high quality
500 giga-ohm seals for single-channel recording using the higher resistance pipettes required for such
501 recordings (Fig. 4). We also found that the viability of the oocytes was greatly reduced following
502 injection of only G375R cRNA, with the oocytes often starting to die by the second or third day

503 after injection, rather than after a week or more, perhaps because a large fraction of the G375R
504 homomeric mutant channels would be expected to be open at resting membrane potentials (Figs.
505 4, 7). These viability problems were not observed for injection of 1:1 mixtures of G375R mutant
506 and WT cRNA, which gave less pronounced negative shifts in activation or for injections of only
507 WT cRNA (Figs. 3, 4, 7),
508 The open probability (Po) of each single channel analyzed in detail was determined for a
509 range of voltages with Clampfit 10.7 using 50% threshold analysis to measure open and closed
510 interval durations. Po at each voltage was calculated by dividing the total open time by the sum
511 of the open and closed times. The durations of recordings to estimate Po ranged from ~ 5 s to ~3
512 min with the time increasing as the Po decreased. For macro patch current recordings, relative
513 conductance was determined from macroscopic tail current amplitudes using the voltage
514 protocols indicated in the figure legends. G/G_{max} vs. V (G-V) plots for macro current recordings
515 and Po vs. V (Po-V) plots for single channels were fitted with a Boltzmann function to estimate
516 V_h, the voltage required for half maximal activation, and *b*, a measure of voltage sensitivity,
517 using
518
519 $$G/G_{max} = 1/(1 + \exp((V_h - V)/b)) \quad (1)$$
520
521 where G/G_{max} is the ratio of conductance to maximum conductance and *b* is the slope factor
522 which gives a measure of voltage sensitivity, where *b* indicates the change in millivolts required
523 to increase G/G_{max} (or Po for single channel recording) *e*-fold at very low G/G_{max} (or Po). Note
524 that an increase in *b* indicates a decrease in slope and voltage sensitivity.
525 Single-channel conductance was determined at 100 mV by setting horizontal cursor lines by
526 eye to the open and closed current levels of single-channel recordings.
527
528 **HEK293 cell culture.** As described previously[53], Human Embryonic Kidney HEK293 cells
529 (ATCC CRL-1573) (ATCC, Manassas, VA) were cultured in Gibco Dulbecco's modified Eagle's
530 medium (DMEM) with 10% fetal bovine serum, 100 units ml^{-1} penicillin and 100 μg ml^{-1}
531 streptomycin (ThermoFisher Scientific, Waltham, MA) and incubated at 37°C with 5% CO_2.
532 These cells were grown and passaged twice a week in T25 flasks (MidSci, St. Louis, MO).
533
534 **Expression of BK channels in HEK293 cells.** HEK293 cells were plated at a density of ~400,000
535 cells per 40 mm petri dish (TPP catalog #93040) a day before transfection. For transfection,
536 plasmid DNA containing cDNA encoding for BK WT and/or BK G375R (mutant) subunits was
537 added to cell layers that were 70-90% confluent using Lipofectamine 2000 transfection reagent
538 (catalog #11668-027, ThermoFisher Scientific, Waltham, MA) following manufacturer's
539 instructions. 2 μg cDNA of WT, mutant, or a mix of WT and mutant (1:1 ratio by weight) was
540 transfected per 40 mm dish. As a marker for transfection, cells were co-transfected with
541 pmaxGFP a CMV plasmid expressing green fluorescent protein (Amaxa Biosystems), at 0.2 μg

542 per dish. After transfection, the cells were incubated at 37°C with 5% CO_2 for 2-4 days until
543 recording. The recordings were then performed at room temperature (22°C). Fluorescent cells
544 were used to study the function of the ion channels that the HEK293 cells were transfected with;
545 non-fluorescing cells were used as a non-transfected controls[54].
546
547 **Whole cell recording from HEK293 cells.** Whole cell recordings were obtained from HEK293
548 cells using an Axopatch 200B amplifier (Molecular Devices, San Jose, CA). Recordings were
549 filtered at 5 kHz with the amplifier internal filter and digitized at 50 kHz using a Digidata 1550B
550 digitizer (Molecular Devices, San Jose, CA). The recording pipette was filled with (in mM): 140
551 KMES, 5 EGTA, 10 HEPES, pH 7.4 with KOH. Bath solutions contained (in mM): 135 NaMES,
552 5 KMES, 1 $MgCl_2$, 10 HEPES, pH 7.4 with NaOH.

553 **Calculating the percentages of the five different stoichiometries of BK channels that can be**
554 **expressed when mimicking a heterozygous mutation.** As shown in Fig. 1, a mutation
555 heterozygous with WT can potentially produce five different types of channels, defined by their
556 stoichiometry. The binomial equation was used to calculate the expected percentages of different
557 combinations of mutant and WT subunits for tetrameric BK channels[29,30]. For the calculations in
558 Fig. 1 this approach assumes that WT and mutant alleles produce equal numbers of mutant and
559 WT subunits that assemble randomly into tetrameric channels of different stoichiometries,
560 labelled assembled channels in Fig. 1, and that each assembled channel has the same probability
561 of being expressed, independent of subunit composition, such that
562
563 $$F_i = (4!((4-i)!\, i!))\, F_{WT}^{(4-i)}\, F_{MUT}^{i} \qquad (2)$$
564
565 where Fi is the fraction of channel types with i mutant subunits, F_{WT} is the fraction of WT cRNA
566 injected, and F_{MUT} is the fraction of mutant cRNA injected, where $F_{WT} + F_{MUT} = 1$. For BK
567 channels, i ranges from 0 to 4, giving five channel types based on subunit composition. Setting
568 both F_{WT} and F_{MUT} to 0.5 gives the fractions of the various channel types for a heterozygous
569 mutation.
570
571 **Simulating the discrete probability distributions of the number of BK channels of each**
572 **stoichiometry expected for equal production and random assembly of mutant and WT**
573 **subunits.** The simulated discrete probability distributions were used to determine if the
574 experimentally observed number of channels of each stoichiometry differed significantly from
575 the number expected for random assembly of mutant and WT subunits. Discrete probability
576 distributions for the five stoichiometries of assembled channels in Fig. 1 for groups of 33
577 channels were simulated as follows. The first step was to generate a group of 33 channels by
578 assuming random assembly of mutant and WT subunits drawn from equal numbers of mutant
579 and WT subunits (with replacement) for each channel in the group. To assemble each channel,

four random numbers between 0 and 1 were drawn. Each random number < 0.5 indicated a WT subunit and each random number ≥ 0.5 indicated a mutant subunit. The number of channels of each of the five stoichiometries for each group of 33 channels were then binned into separate histograms for each stoichiometry. This process was then repeated for 10^6 groups of 33 channels. Each histogram of the numbers of channels of each type for the 10^6 groups was then normalized to a discrete probability distribution with a summed probability of 1.0, to indicate the probability of observing the indicated number of channels of that stoichiometry in a group of 33 channels. These predicted discrete probability distributions are presented in Supplementary Fig. 4 for comparison to the experimentally observed number indicated by red histogram bars in the same figure.

Software. The computer program for simulating the discrete probability distributions for the different types of channels assuming random assembly of mutant and WT subunits, Binomdouble4-33.bas, is written in QB64 and is available from the corresponding author upon request. The increments of single channel conductance and V_h added by each G375R mutant and WT subunit for Figs. 5C and 6D were optimized by minimizing the least squared differences between the experimental values and those calculated with the equations in the legends of Figs. 5 and 6 by running Solver in Excel.

Statistics. Error bars in the figures and error estimates in the text are SEM. Significance was determined with the two-tailed *t*-test unless otherwise indicated.

Data Availability. The data for this study are contained in the figures and text of the manuscript and the Supplementary information.

606 **References**

607 1. Barrett, J.N., Magleby, K.L. & Pallotta, B.S. Properties of single calcium-activated potassium
608 channels in cultured rat muscle. *J. Physiol* **331**, 211-230 (1982).
609 2. Latorre, R., Vergara, C. & Hidalgo, C. Reconstitution in planar lipid bilayers of a Ca2+-dependent K+
610 channel from transverse tubule membranes isolated from rabbit skeletal muscle. *Proc. Natl. Acad.*
611 *Sci. U. S. A* **79**, 805-809 (1982).
612 3. McCobb, D.P. *et al.* A human calcium-activated potassium channel gene expressed in vascular
613 smooth muscle. *Am. J. Physiol* **269**, H767-H777 (1995).
614 4. Rothberg, B.S. & Magleby, K.L. Voltage and Ca2+ activation of single large-conductance Ca2+-
615 activated K+ channels described by a two-tiered allosteric gating mechanism. *J. Gen. Physiol* **116**,
616 75-99 (2000).
617 5. Horrigan, F.T. & Aldrich, R.W. Coupling between voltage sensor activation, Ca2+ binding and
618 channel opening in large conductance (BK) potassium channels. *J. Gen. Physiol* **120**, 267-305
619 (2002).
620 6. Xia, X.M., Zeng, X. & Lingle, C.J. Multiple regulatory sites in large-conductance calcium-activated
621 potassium channels. *Nature* **418**, 880-884 (2002).
622 7. Salkoff, L., Butler, A., Ferreira, G., Santi, C. & Wei, A. High-conductance potassium channels of the
623 SLO family. *Nat. Rev. Neurosci* **7**, 921-931 (2006).
624 8. Horrigan, F.T. Perspectives on: conformational coupling in ion channels: conformational coupling
625 in BK potassium channels. *J. Gen. Physiol* **140**, 625-634 (2012).
626 9. Geng, Y. & Magleby, K.L. Single-channel kinetics of BK (Slo1) channels. *Front Physiol* **5**, 532 (2014).
627 10. Pantazis, A. & Olcese, R. Biophysics of BK Channel Gating. *Int. Rev. Neurobiol* **128**, 1-49 (2016).
628 11. Latorre, R. *et al.* Molecular Determinants of BK Channel Functional Diversity and Functioning.
629 *Physiol Rev* **97**, 39-87 (2017).
630 12. Zhou, Y., Yang, H., Cui, J. & Lingle, C.J. Threading the biophysics of mammalian Slo1 channels onto
631 structures of an invertebrate Slo1 channel. *J. Gen. Physiol* **149**, 985-1007 (2017).
632 13. Tao, X., Hite, R.K. & MacKinnon, R. Cryo-EM structure of the open high-conductance Ca(2+)-
633 activated K(+) channel. *Nature* **541**, 46-51 (2017).
634 14. Hite, R.K., Tao, X. & MacKinnon, R. Structural basis for gating the high-conductance Ca(2+)-
635 activated K(+) channel. *Nature* **541**, 52-57 (2017).
636 15. Tao, X. & MacKinnon, R. Molecular structures of the human Slo1 K(+) channel in complex with
637 beta4. *Elife* **8**(2019).
638 16. Geng, Y. *et al.* Coupling of Ca(2+) and voltage activation in BK channels through the alphaB
639 helix/voltage sensor interface. *Proc Natl Acad Sci U S A* **117**, 14512-14521 (2020).
640 17. Brenner, R. *et al.* Vasoregulation by the beta1 subunit of the calcium-activated potassium channel.
641 *Nature* **407**, 870-876 (2000).
642 18. Robitaille, R., Garcia, M.L., Kaczorowski, G.J. & Charlton, M.P. Functional colocalization of calcium
643 and calcium-gated potassium channels in control of transmitter release. *Neuron* **11**, 645-655
644 (1993).
645 19. Harvey, J.R.M., Plante, A.E. & Meredith, A.L. Ion Channels Controlling Circadian Rhythms in
646 Suprachiasmatic Nucleus Excitability. *Physiol Rev* **100**, 1415-1454 (2020).
647 20. Gu, N., Vervaeke, K. & Storm, J.F. BK potassium channels facilitate high-frequency firing and cause
648 early spike frequency adaptation in rat CA1 hippocampal pyramidal cells. *J Physiol* **580**, 859-882
649 (2007).
650 21. Park, S.M. *et al.* BK channel properties correlate with neurobehavioral severity in three KCNMA1-
651 linked channelopathy mouse models. *Elife* **11**(2022).

652 22. Montgomery, J.R. & Meredith, A.L. Genetic activation of BK currents in vivo generates
653 bidirectional effects on neuronal excitability. *Proc Natl Acad Sci U S A* **109**, 18997-9002 (2012).
654 23. Wang, B., Rothberg, B.S. & Brenner, R. Mechanism of increased BK channel activation from a
655 channel mutation that causes epilepsy. *J. Gen. Physiol* **133**, 283-294 (2009).
656 24. Yang, J. *et al.* An epilepsy/dyskinesia-associated mutation enhances BK channel activation by
657 potentiating Ca2+ sensing. *Neuron* **66**, 871-883 (2010).
658 25. Liang, L. *et al.* De novo loss-of-function KCNMA1 variants are associated with a new multiple
659 malformation syndrome and a broad spectrum of developmental and neurological phenotypes.
660 *Hum Mol Genet* **28**, 2937-2951 (2019).
661 26. Bailey, C.S., Moldenhauer, H.J., Park, S.M., Keros, S. & Meredith, A.L. KCNMA1-linked
662 channelopathy. *J Gen Physiol* **151**, 1173-1189 (2019).
663 27. Miller, J.P., Moldenhauer, H.J., Keros, S. & Meredith, A.L. An emerging spectrum of variants and
664 clinical features in KCNMA1-linked channelopathy. *Channels (Austin)* **15**, 447-464 (2021).
665 28. Cui, J. BK Channel Gating Mechanisms: Progresses Toward a Better Understanding of Variants
666 Linked Neurological Diseases. *Front Physiol* **12**, 762175 (2021).
667 29. MacKinnon, R. Determination of the subunit stoichiometry of a voltage-activated potassium
668 channel. *Nature* **350**, 232-235 (1991).
669 30. Blaine, J.T. & Ribera, A.B. Heteromultimeric potassium channels formed by members of the Kv2
670 subfamily. *J Neurosci* **18**, 9585-93 (1998).
671 31. Niu, X. & Magleby, K.L. Stepwise contribution of each subunit to the cooperative activation of BK
672 channels by Ca2+. *Proc Natl Acad Sci U S A* **99**, 11441-6 (2002).
673 32. Bergendahl, L.T. *et al.* The role of protein complexes in human genetic disease. *Protein Sci* **28**,
674 1400-1411 (2019).
675 33. Backwell, L. & Marsh, J.A. Diverse Molecular Mechanisms Underlying Pathogenic Protein
676 Mutations: Beyond the Loss-of-Function Paradigm. *Annu Rev Genomics Hum Genet* **23**, 475-498
677 (2022).
678 34. Chen, X., Yan, J. & Aldrich, R.W. BK channel opening involves side-chain reorientation of multiple
679 deep-pore residues. *Proc. Natl. Acad. Sci. U. S. A* **111**, E79-E88 (2014).
680 35. Hamill, O.P., Marty, A., Neher, E., Sakmann, B. & Sigworth, F.J. Improved patch-clamp techniques
681 for high-resolution current recording from cells and cell-free membrane patches. *Pflugers Arch*
682 **391**, 85-100 (1981).
683 36. Niu, X. & Magleby, K.L. Stepwise contribution of each subunit to the cooperative activation of BK
684 channels by Ca2+. *Proc. Natl. Acad. Sci. U. S. A* **99**, 11441-11446 (2002).
685 37. Gonzalez-Perez, V., Xia, X.M. & Lingle, C.J. Two classes of regulatory subunits coassemble in the
686 same BK channel and independently regulate gating. *Nat. Commun* **6**, 8341 (2015).
687 38. Miller, D.C., Weinstock, M.M. & Magleby, K.L. Is the quantum of transmitter release composed of
688 subunits? *Nature* **274**, 388-390 (1978).
689 39. McManus, O.B. & Magleby, K.L. Accounting for the Ca(2+)-dependent kinetics of single large-
690 conductance Ca(2+)-activated K+ channels in rat skeletal muscle. *J. Physiol* **443**, 739-777 (1991).
691 40. Brelidze, T.I., Niu, X. & Magleby, K.L. A ring of eight conserved negatively charged amino acids
692 doubles the conductance of BK channels and prevents inward rectification. *Proc. Natl. Acad. Sci. U.*
693 *S. A* **100**, 9017-9022 (2003).
694 41. Nimigean, C.M., Chappie, J.S. & Miller, C. Electrostatic tuning of ion conductance in potassium
695 channels. *Biochemistry* **42**, 9263-9268 (2003).
696 42. Geng, Y., Niu, X. & Magleby, K.L. Low resistance, large dimension entrance to the inner cavity of BK
697 channels determined by changing side-chain volume. *J. Gen. Physiol* **137**, 533-548 (2011).
698 43. Friedrich, C. *et al.* Gain-of-function mutation in TASK-4 channels and severe cardiac conduction
699 disorder. *EMBO Mol Med* **6**, 937-51 (2014).

44. Du, X. *et al.* Loss-of-function BK channel mutation causes impaired mitochondria and progressive cerebellar ataxia. *Proc Natl Acad Sci U S A* **117**, 6023-6034 (2020).
45. Fink, M. *et al.* Dominant negative chimeras provide evidence for homo and heteromultimeric assembly of inward rectifier K+ channel proteins via their N-terminal end. *FEBS Lett* **378**, 64-68 (1996).
46. Ribera, A.B., Pacioretty, L.M. & Taylor, R.S. Probing molecular identity of native single potassium channels by overexpression of dominant negative subunits. *Neuropharmacology* **35**, 1007-1016 (1996).
47. Silberberg, S.D., Chang, T.H. & Swartz, K.J. Secondary structure and gating rearrangements of transmembrane segments in rat P2X4 receptor channels. *J Gen Physiol* **125**, 347-59 (2005).
48. Hichri, E., Selimi, Z. & Kucera, J.P. Modeling the Interactions Between Sodium Channels Provides Insight Into the Negative Dominance of Certain Channel Mutations. *Front Physiol* **11**, 589386 (2020).
49. Reed, A.P., Bucci, G., Abd-Wahab, F. & Tucker, S.J. Dominant-Negative Effect of a Missense Variant in the TASK-2 (KCNK5) K+ Channel Associated with Balkan Endemic Nephropathy. *PLoS One* **11**, e0156456 (2016).
50. Wang, Y.W., Ding, J.P., Xia, X.M. & Lingle, C.J. Consequences of the stoichiometry of Slo1 alpha and auxiliary beta subunits on functional properties of large-conductance Ca2+-activated K+ channels. *J. Neurosci* **22**, 1550-1561 (2002).
51. Gonzalez-Perez, V., Ben, J.M., Xia, X.M. & Lingle, C.J. Regulatory gamma1 subunits defy symmetry in functional modulation of BK channels. *Proc. Natl. Acad. Sci. U. S. A* **115**, 9923-9928 (2018).
52. Gonzalez-Perez, V., Xia, X.M. & Lingle, C.J. Functional regulation of BK potassium channels by gamma1 auxiliary subunits. *Proc. Natl. Acad. Sci. U. S. A* **111**, 4868-4873 (2014).
53. Santi, C.M. *et al.* Opposite regulation of Slick and Slack K+ channels by neuromodulators. *J. Neurosci* **26**, 5059-5068 (2006).
54. Han, Y., Li, P. & Slaughter, M.M. Selective antagonism of rat inhibitory glycine receptor subunits. *J Physiol* **554**, 649-58 (2004).
55. Ding, J.P., Li, Z.W. & Lingle, C.J. Inactivating BK channels in rat chromaffin cells may arise from heteromultimeric assembly of distinct inactivation-competent and noninactivating subunits. *Biophys. J* **74**, 268-289 (1998).

Acknowledgements This work was supported in part by NIH grant R01-GM114694 to L.S. and K.L.M. We thank Julia Bulova for technical help during the initial phase of this project.

Author contributions

Y.G., P.L., L.S., and K.L.M. designed research; Y.G., P.L., A.B., B.W., L.S., and K.L.M performed research; L.S. and K.L.M. wrote the manuscript with input from the other authors.

Competing interests

The authors declare no competing interests.

Additional information

Supplementary information is included.

Correspondence and requests for materials can be addressed to Lawrence Salkoff (salkoffl@wustl.edu) or Karl L. Magleby (kmagleby@miami.edu).

743

744 **Figure legends**

745

746 **Fig. 1 Protein subunits encoded by WT and mutant alleles for a heterozygous mutation could**
747 **potentially assemble into five different stoichiometries of tetrameric BK channels and six**
748 **different subunit arrangements**[29,30,32,36,55]**.** In this diagram, WT and mutant alleles (left) encode
749 for WT and mutant protein subunits (middle), which then assemble into tetrameric assembled
750 channels with five different subunit stoichiometries and six different subunit arrangements
751 (right). The listed theoretical frequencies of expression of the five different stoichiometries of
752 assembled channels were calculated with Eqn. 2 in the Methods, which assumes that equal
753 numbers of mutant and WT subunits randomly assemble into tetrameric channels, each with
754 equal probability of reaching the surface membrane. With random assembly, ~6% of the
755 assembled channels are WT comprised of four WT subunits per channel, ~88% are hybrid
756 (mixed subunit) channels with from 1 to 3 mutant subunits per channel, and ~6% are
757 homomeric mutant channels comprised of four mutant subunits per channel. Note that ~94%
758 of the assembled channels can be pathogenic, as they contain from 1 to 4 mutant subunits per
759 channel. The listed percentages of ~6%, ~38%, and ~94% here and throughout the paper have
760 been rounded from the calculated values of 6.25%, 37.5%, and 93.75%. The 37.5% reflects the
761 sum of 25% for hybrid channels with two adjacent mutant subunits and 12.5% for hybrid
762 channels with two diagonal mutant subunits[32]. For experimentation, assembled channels are
763 those channels expressed following injection of a 1:1 mixture of mutant and WT cRNA into
764 *Xenopus* oocytes, to mimic a mutation in which the mutant allele is heterozygous with the WT
765 allele.

766

767 **Fig. 2 BK channels expressed in oocytes following injection of a 1:1 mixture of G375R mutant**
768 **and WT cRNA activate at greatly left shifted negative potentials compared to BK channels**
769 **expressed following injection of only WT cRNA.** (***A***) Whole cell currents recorded from oocytes
770 with the two-electrode voltage clamp for the indicated injections of cRNA. The whole cell
771 currents were generated by holding the potential at -80 mV and then jumping to voltages
772 ranging from -140 mV to +60 mV in 10 mV increments (1:1) or to +100 mV (WT and Blank). (***B***)
773 Plots of relative conductance versus the voltage of the steps following: injection of: a 1:1
774 mixture of mutant and WT cRNA (red diamonds); injection of WT cRNA alone (black circles); or
775 injection of carrier only (purple triangles). The high conductance at negative potentials would
776 act to drive the membrane potential to about -80 mV, the equilibrium potential of K^+. Channel
777 activation is left shifted in the whole cell recordings in this figure compared to the ~0 Ca^{2+}
778 macro patch recordings in Fig. 3, because the resting free Ca^{2+} in the oocytes of a few

779 micromolar left shifts BK channel activation. The relative cord conductance was calculated from
780 the plotted steady-state currents in Supplementary Fig. 2 using the step potential minus the
781 reversal potential for the voltage driving force. Mean ± SEM, n = 4 in each case.
782
783 **Fig. 3 Quantifying the mean negative shift in V_h following injection of a 1:1 mixture of G375R**
784 **mutant and WT cRNA when compared to injection of only WT cRNA.** Data are for essentially 0
785 Ca^{2+} at the intracellular side of the membrane. (***A***) Currents recorded from inside-out macro
786 patches of membrane excised from oocytes. For WT channels following injection of only WT
787 cRNA, holding potential was -80 mV and voltage pulses were from -80 mV to 240 mV with 20
788 mV steps followed by a step back to -80 mV to elicit tail currents for G/Gmax measurements.
789 For channels expressed following injection of a 1:1 mixture of G375R mutant and WT cRNA,
790 holding potential was -160 mV and voltage pulses were from -120 to 240 mV with 20 mV steps
791 followed by a step back to -120 mV to elicit tail current for measurement. The currents are the
792 mean response from the many hundreds to thousands of BK channels in each excised macro
793 patch of membrane. (***B***) G/G_{max} vs. voltage plots following the injection of WT cRNA alone
794 (black circles, n = 6), or 1:1 injection of mutant and WT cRNA (red diamonds, n = 12). The black
795 line through the WT data is a single Boltzmann function with V_h = 181.3 mV and slope factor *b* =
796 24.04 mV/e-fold change in Po at low Po. The blue line through the 1:1 data (red diamonds) is a
797 single Boltzmann function with V_h = 59.04 mV and *b* = 38.06 mV/e-fold change. The red line
798 through the 1:1 data is the sum of five Boltzmann functions with: 1) V_h = -75.7 mV, *b* =21.6
799 mV/e-fold change, fractional area = 0.0547; 2) 1.5, 21.0, 0.236; 3) 54.6, 13.8, 0.316; 4) 96.6,
800 14.4, 0.244; 5) 155, 14.0, 0.139. These parameters for the five summed Boltzmann functions
801 that describe the 1:1 data are generally consistent with the V_h values for the apparent clusters
802 of assembled channels (Fig. 5A) and theoretical percentages in Fig. 1.
803
804 **Fig. 4 Identifying the types of assembled BK channels expressed following a 1:1 injection of**
805 **G375R mutant and WT cRNA.** (***A***) Representative single channel recordings from three different
806 single BK channel molecules: WT channel (top row) following injection of WT cRNA; an
807 assembled channel following 1:1 injection of G375R mutant and WT cRNA, (second row); and a
808 G375R homomeric mutant channel following injection of G375R mutant cRNA (third row).
809 Recordings are shown at three different voltages for each channel type. Depolarization
810 activates each channel type with a markedly different V_h of 140 mV for the WT channel, 6 mV
811 for the assembled channel, and -100 mV for the G375R homomeric mutant channel. Arrows
812 indicate closed channel current levels. (***B***) Plots of Po vs. *V* for 33 individual assembled channels
813 following a 1:1 injection of mutant and WT cRNA (red diamonds with Boltzmann fits). (***C***) Plots
814 of Po vs. *V* for 12 single G375R homomeric mutant channels following injection of G375R
815 mutant cRNA (blue squares with Boltzmann fits), and for 9 WT channels following injection of

816 WT cRNA (black circles and Boltzmann fits). (***D***) Identifying the types of assembled channels.
817 Blue and gray areas indicate the range of observed V_h values for G375R homomeric mutant
818 channels and WT channels, respectively, from *C*. One of the assembled channels (rightmost red
819 Po-*V* curve) overlaps with the WT channels (gray shading), indicating that this assembled
820 channel is likely a WT channel with four WT subunits. Four of the assembled channels (four
821 leftmost red Po-*V* curves) overlap with the G375R homomeric mutant channels (blue shading)
822 indicating that these four assembled channels are likely G375R homomeric mutant channels
823 assembled from four mutant subunits. The remaining 28 assembled channels would be hybrid
824 channels with mixed subunits (Fig. 1), as their V_h values do not overlap with those of either
825 homomeric mutant or WT channels.
826
827
828 **Fig. 5 Five different types of functional BK channels are observed following injection of a 1:1**
829 **mixture of mutant and WT cRNA into *Xenopus* oocytes.** ***(A)*** Histograms of V_h values of single
830 channels from Fig. 4. WT channels expressed after injection of only WT cRNA are indicated by
831 black bars, and G375R homomeric mutant channels expressed after injection of only G375R
832 cRNA are indicated by blue bars. Assembled channels expressed after a 1:1 injection of mutant
833 and WT cRNA are indicated by red bars. The red bar in the cluster of black bars is an assembled
834 channel comprised of four WT subunits. The four red bars interspaced between the blue bars
835 are assembled channels comprised of four mutant subunits. The 28 red bars with V_h values in
836 between the blue bars and black bars are hybrid assembled channels of mixed subunits. The
837 hybrid channels appear to cluster into three groups with mean V_h values of 1.4, 59 and 96 mV.
838 Hypothesized subunit compositions of the three apparent clusters of hybrid channels are
839 indicated, where black indicates WT subunits and blue indicates G375R mutant subunits. (***B***)
840 The experimentally observed frequencies of the five types of assembled channels are listed for
841 comparison to the theoretical frequencies in Fig. 1. (***C***) V_h for the five types of assembled
842 channels is approximated by a linear incremental model where each subunit contributes an
843 increment of V_h,

844 $$V_h(N_M) = N_M\ (-16.7\ \text{mV}) + (4-N_M)\ 40.5\ \text{mV},$$

845 where N_M is the number of G375R mutant subunits per channel, $V_h(N_M)$ is V_h as a function of
846 N_M, and -16.7 mV and 40.5 mV are the increments of V_h added by each mutant and WT subunit,
847 respectively. Filled red circles are the experimentally observed mean ± SEM values of V_h for the
848 five types of assembled channels from part *A*, and the dashed line indicates the predicted
849 values. Predictions are for 0 intracellular Ca^{2+}. Mean ± SEM. Histograms of single-channel
850 kinetic parameters have been used previously to investigate the number of β2 regulatory
851 subunits per BK channel[50].

852
853
854 **Fig. 6 Each replacement of a WT subunit with a G375R mutant subunit in a BK channel acts to**
855 **both left shift V_h to more negative potentials and decrease single channel conductance.** (***A***)
856 Single-channel currents recorded from single channels at +100 mV after injecting the indicated
857 cRNA. (***B***) Single-channel conductance at +100 mV decreases as the number of mutant subunits
858 increase. Mean single-channel conductance for WT channels was 312 ± 4 pS (n = 7), decreasing
859 to 245 ± 6 pS for hybrid channels (n = 25, $p < 0.0001$), and further decreasing to 190 ± 14 pS for
860 G375R homomeric mutant channels (n = 8, p = 0.0003). Mean ± SEM. WT and G375R
861 homomeric mutant channels were those channels expressed after injecting only WT cRNA or
862 only G375R mutant cRNA, respectively. Hybrid channels were identified as in Fig. 4D. (***C***) Plot of
863 single channel conductance at +100 mV vs. V_h for BK channels expressed following injection of
864 the indicated cRNA. The linear regression line plots single channel conductance g vs. V_h, where:
865 $g = g(0) + aV$, where $g(0)$ = 231.9 ± 3.9 pA and a = 0.408 ± 0.0375 pS/mV ($p < 0.0001$ for slope
866 significantly different from 0. R = 0.86). (***D***) Single channel conductance for the five types of
867 assembled channels is predicted by a linear incremental model, where each subunit contributes
868 an increment of conductance,

869 $$g(N_M) = N_M\ 46.1\ \text{pS} + (4-N_M)\ 76.5\ \text{pS},$$

870 where N_M is the number of G375R mutant subunits per channel, $g(N_M)$ is single channel
871 conductance as a function of N_M, and 46.1 pS and 76.5 pS are the increments of g added by
872 each mutant and WT subunit, respectively. The homomeric mutant and WT data are from part
873 *B*, and the three red hybrid conductance bars plot g from the three groups of hybrid channels in
874 Fig. 5A. The red dashed line indicates the predicted values of g. Mean ± SEM.
875
876
877 **Fig. 7 G375R homomeric mutant channels, assembled channels, and WT BK channels are**
878 **expressed in HEK293 cells.** (***A***) Whole cell currents recorded from HEK293 cells following
879 transfection with the indicated types of cDNA. The whole cell currents were generated by
880 holding at -60 mV, with a pre-step to -100 mV, followed by steps from −200 or −100 to +200 mV
881 in 10 mV increments followed by a post-step to -120 mV. The dashed line indicates the level of
882 0 current. Evoked currents were not observed in HEK293 cells that were not transfected. (***B***)
883 Plots of normalized conductance versus the voltage of the activating steps following
884 transfections with G375R mutant cDNA (blue squares), a 1:1 mixture of mutant and WT cDNA
885 (red diamonds) to express assembled channels, or WT cDNA (black circles). Unlike single
886 channel recordings (Fig. 4), whole cell recordings reflect the average response from many
887 hundreds to thousands of channels. There were large negative shifts in V_h for G/Gmax curves

determined from G375R homomeric mutant channels and from assembled channels, when compared to WT channels. The mean voltage for half activation (V_h) was 130.3 ± 4.4 mV (n = 4) for WT BK currents, 37.5 ± 2.7 mV (n = 5) for BK currents from the 1:1 injection, and -142.5 ± 3.6 mV (n = 3) for the G375R homomeric mutant channels. The 1:1 transfection also decreased the voltage sensitivity of activation compared to WT, with a slope of 52.0 ± 2.0 mV (n = 5) per e-fold change for current after a 1:1 transfection, compared to 32.3 ± 2.5 mV (n = 4) for WT currents. The G375R homomeric mutant channels had a slope of 45.0 ± 4.0 mV. Mean ± SEM.

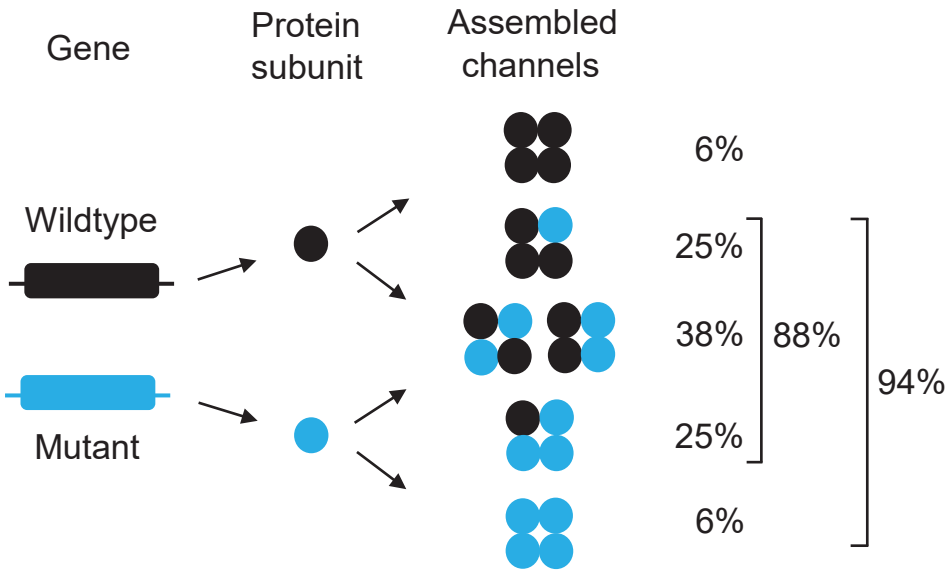
Gene
Protein subunit
Assembled channels
Wildtype
Mutant
6%
25%
38%
25%
6%
88%
94%

Figure 1

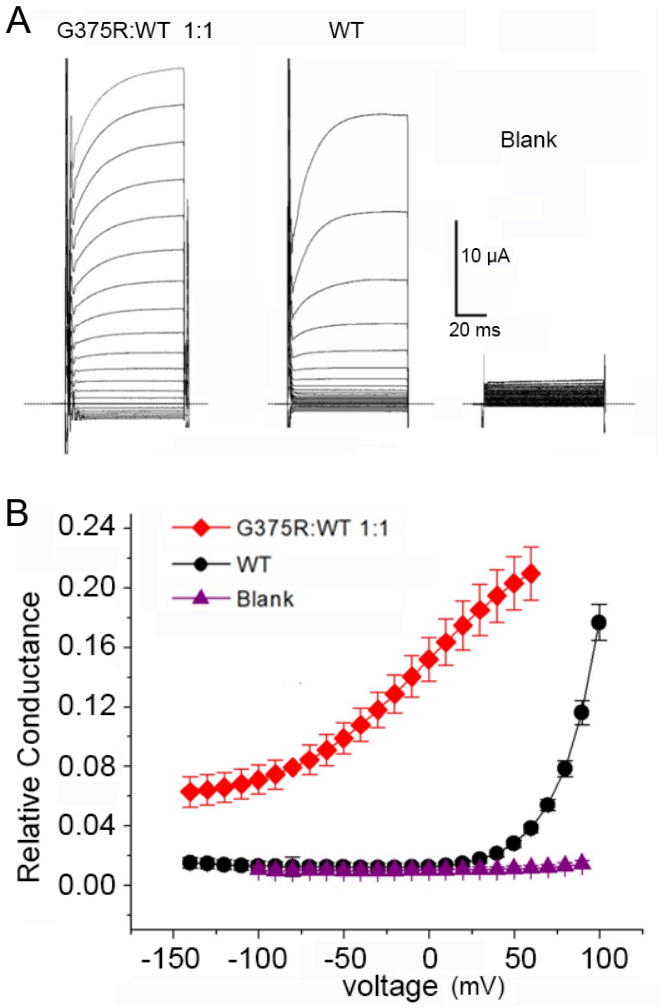
A
G375R:WT 1:1
WT
Blank
10 µA
20 ms
B
G375R:WT 1:1
WT
Blank
Relative Conductance
0.24
0.20
0.16
0.12
0.08
0.04
0.00
-150
-100
-50
0
50
100
voltage (mV)

Figure 2

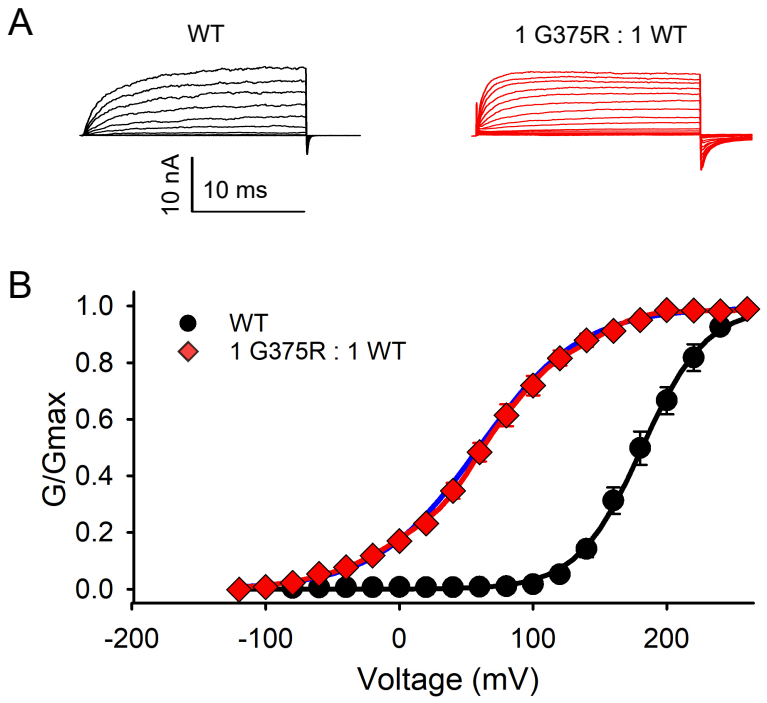
A
WT
1 G375R : 1 WT
10 nA
10 ms
B
WT
1 G375R : 1 WT
G/Gmax
1.0
0.8
0.6
0.4
0.2
0.0
-200
-100
0
100
200
Voltage (mV)

Figure 3

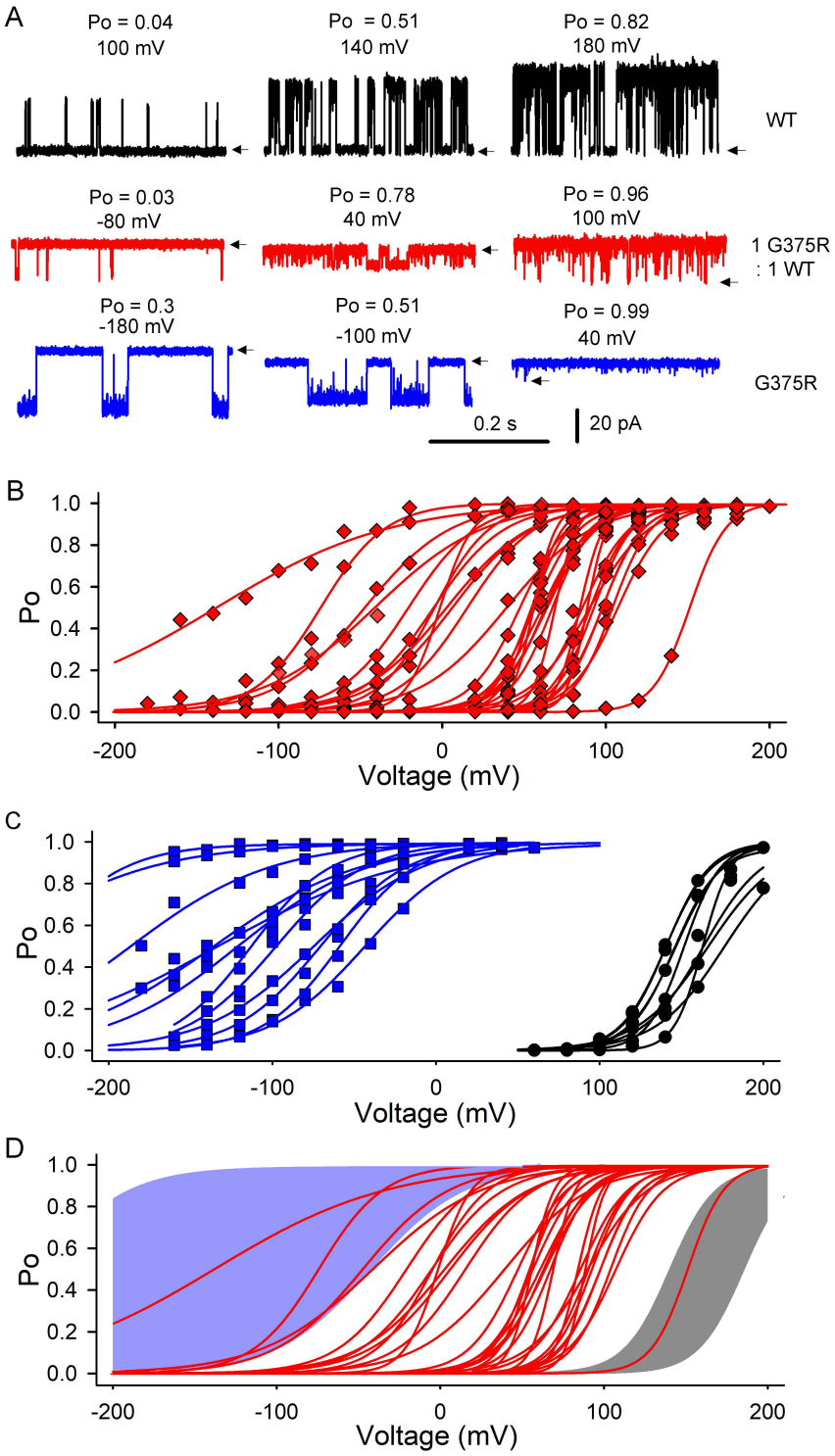
A
Po = 0.04
100 mV
Po = 0.51
140 mV
Po = 0.82
180 mV
WT
Po = 0.03
-80 mV
Po = 0.78
40 mV
Po = 0.96
100 mV
1 G375R
: 1 WT
Po = 0.3
-180 mV
Po = 0.51
-100 mV
Po = 0.99
40 mV
G375R
0.2 s
20 pA
B
Po
Voltage (mV)
C
Po
Voltage (mV)
D
Po
Voltage (mV)

Figure 4

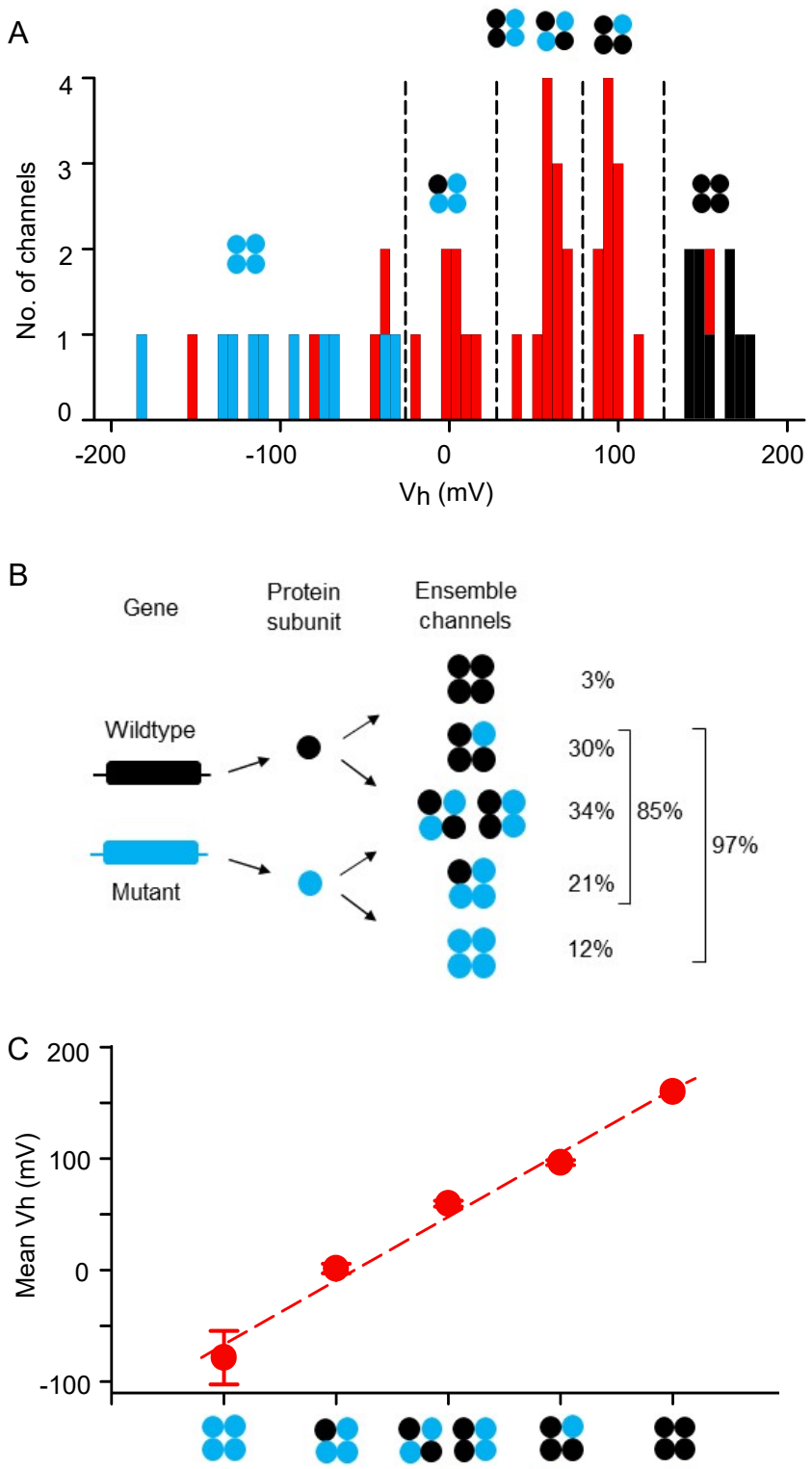
A
No. of channels
4
3
2
1
0
-200
-100
0
100
200
Vh (mV)
B
Gene
Protein subunit
Ensemble channels
Wildtype
Mutant
3%
30%
34%
21%
12%
85%
97%
C
Mean Vh (mV)
200
100
0
-100

Figure 5

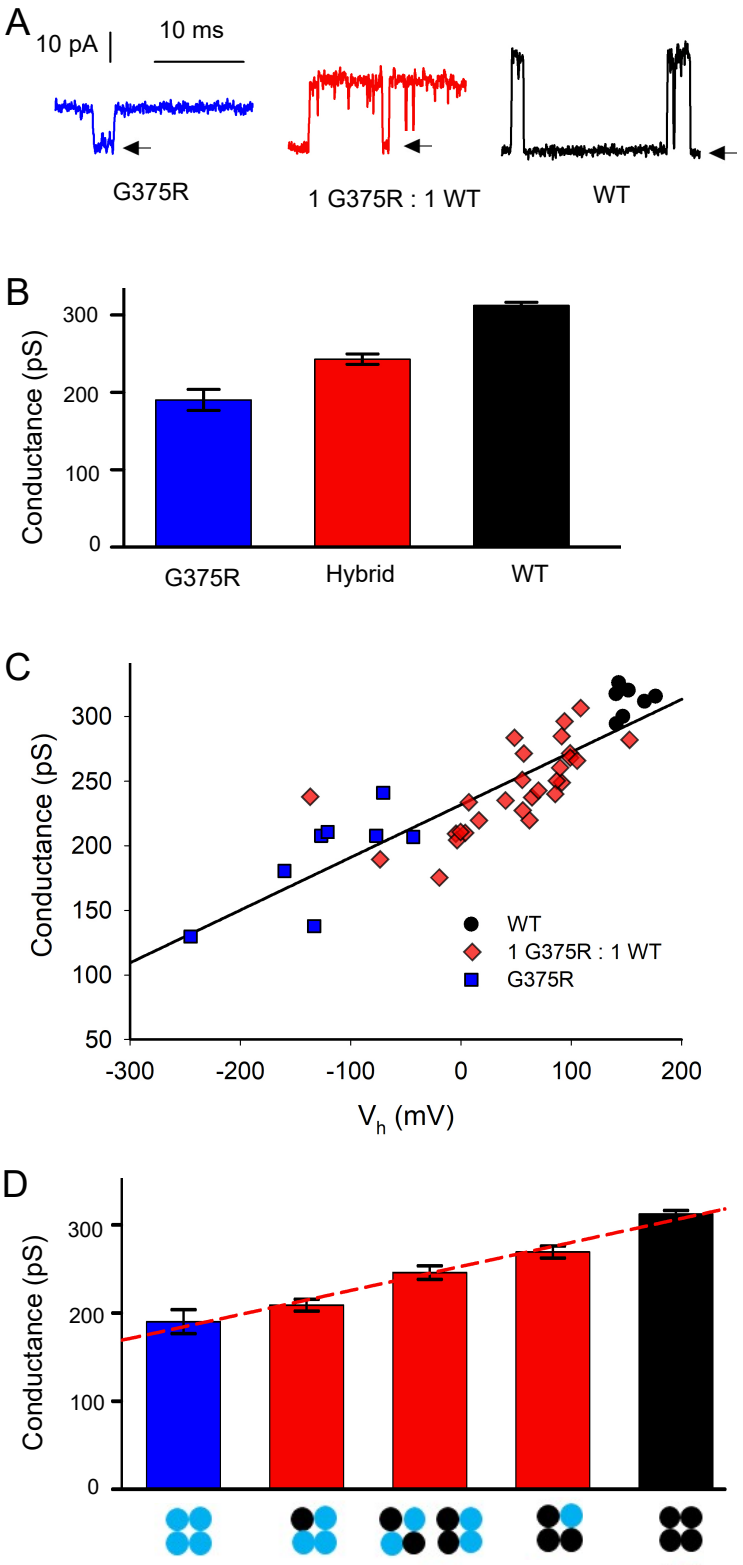
A
10 pA
10 ms
G375R
1 G375R : 1 WT
WT
B
Conductance (pS)
300
200
100
0
G375R
Hybrid
WT
C
Conductance (pS)
300
250
200
150
100
50
-300
-200
-100
0
100
200
V_h (mV)
WT
1 G375R : 1 WT
G375R
D
Conductance (pS)
300
200
100
0

Figure 6

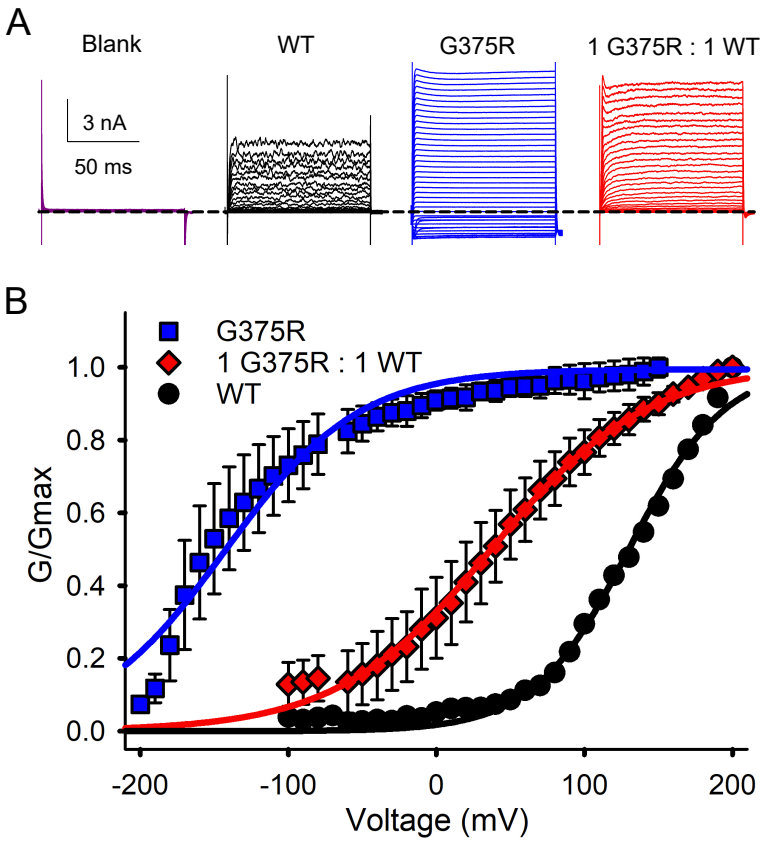
A
Blank
WT
G375R
1 G375R : 1 WT
3 nA
50 ms
B
G375R
1 G375R : 1 WT
WT
G/Gmax
1.0
0.8
0.6
0.4
0.2
0.0
-200
-100
0
100
200
Voltage (mV)

Figure 7

899 **nature communications**

900 **Supplementary information**

901 BK channels of five different subunit combinations underlie the 902 *de novo* KCNMA1 G375R channelopathy

903 Yanyan Geng, Ping Li, Alice Butler, Bill Wang, Lawrence Salkoff, and Karl L. Magleby

904 Contents: Supplementary Figs. 1-4

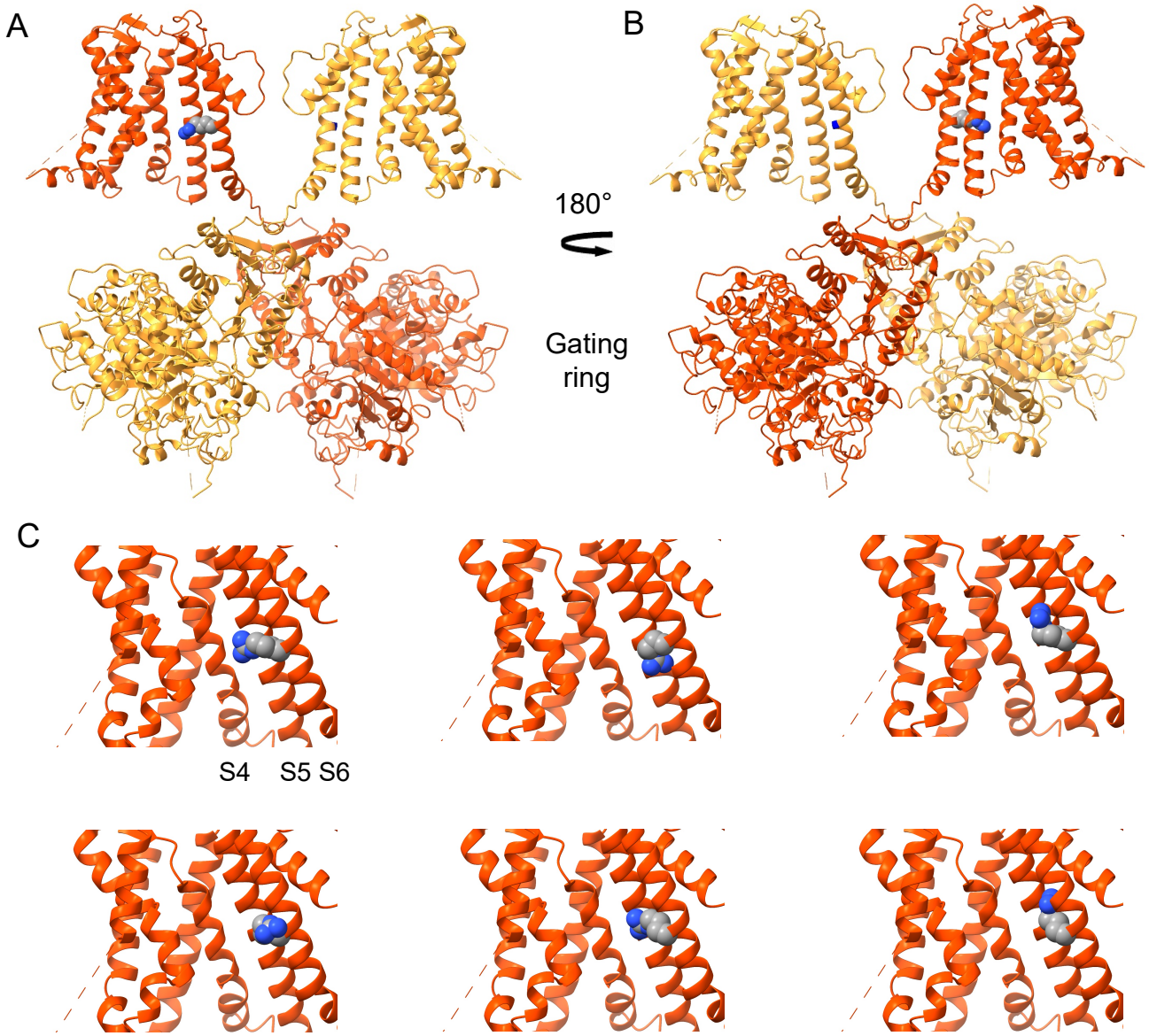

Supplementary Fig. 1 Cryo-EM ribbon structures of the Ca^{2+}-free human BK channel (PDB ID:6V3G)[1] showing the location of the mutant arginine side chain G375R. (***A***) BK channel structure with the front and back (pore-forming alpha) subunits removed. The arginine side chain of the G375R mutation is shown in space filling format on the back side of S6 away from the conduction pathway on the red colored subunit. Carbon atoms are gray, nitrogen blue and hydrogen not indicated. (***B***) Structure after rotating 180° so that the location (blue mark) of the WT glycine side chain of G375 is visible on the back side of S6 on the yellow subunit. (***C***) Six possible orientations of the mutant arginine side chain are shown, generated by ChimeraX software www.cgl.ucsf.edu/chimerax. The mutation G375D (G310D in the referenced publication) also produces a left shift in activation[2] as G375R does, but of half the magnitute. This raises the possibility that the left shift may be related to the bulk of the substituted side chain rather than the specific charge, which is reversed for these two mutations.

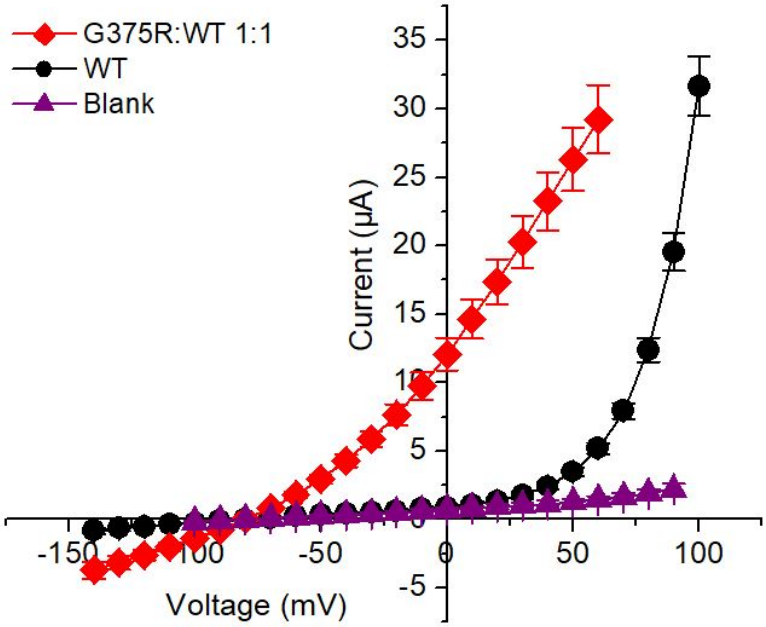

919 **Supplementary Fig. 2 BK currents in *Xenopus* oocytes following injection of a 1:1 mixture**
920 **of G375R mutant and WT cRNA activate at greatly left shifted negative**
921 **voltages compared to BK currents following injection of only WT cRNA.** I-V plots for
922 the indicated injections of cRNA and blank. Two-electrode whole cell voltage clamp. These
923 currents were used to calculate the relative conductance plotted in Fig. 2. Protocol
924 details are in Fig. 2 legend. The amount of WT cRNA injected was 25 times greater than
925 for the injection of the 1:1 mixture of G375R mutant and WT cRNA, so that the initial
926 deviation of WT currents from the baseline could be readily detected.

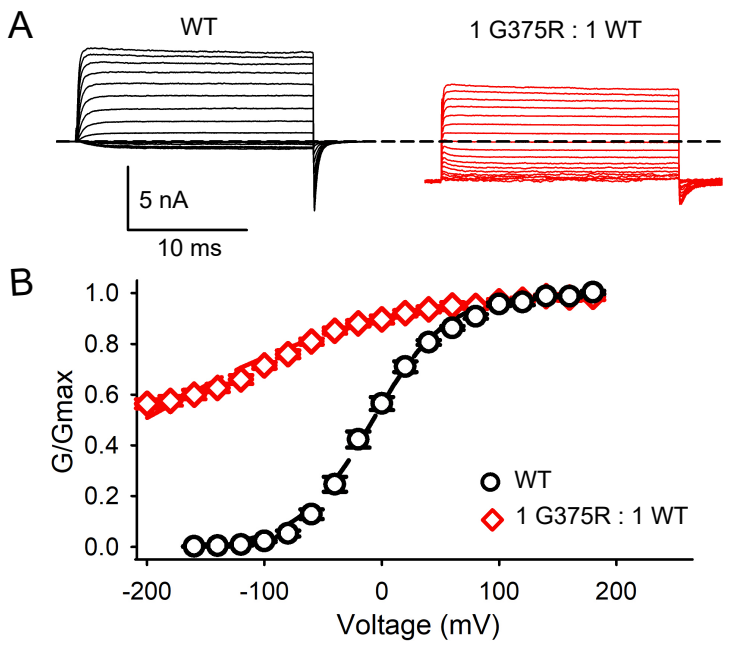

927 **Supplementary Fig. 3 The aberrant negative shift in V_h for BK currents expressed following**
928 **a 1:1 injection of G375R mutant and WT cRNA is also observed with 300 µM intracellular**
929 **Ca^{2+}.** (***A***) Currents recorded from inside-out macro patches of membrane with 300 µM Ca^{2+} at
930 the inner membrane surface. For WT channels voltage pulses were from -160 mV to 180 mV
931 with 20 mV steps from a holding potential of -160 mV. Conductance was measured from tail
032 currents after stepping to -160 mV. For channels expressed following injection of a 1:1
933 mixture of G375R mutant and WT cRNA, voltage pulses were from -200 mV to 180 mV with
934 20 mV steps from a holding potential of -200 mV. Conductance was measured from tail
935 currents after stepping to -200 mV. The dashed line indicates the level of 0 current. In the
936 presence of 300 µM intracellulear Ca^{2+}, more than half of the channels expressed following
937 the 1:1 injection of G375R mutant and WT cRNA remain open at -200 mV. The macro
938 currents are the average response from many hundreds of BK channels in each macro patch.
939 (***B***) G/Gmax vs. voltage plots following injection of WT cRNA alone (black circles) or a 1:1
940 injection of mutant and WT cRNA (red diamonds). The mean voltage for half activation V_h for
941 WT currents was -7.2 ± 3.3 mV, shifting to -205 ± 9.6 mV for BK currents expressed from a 1:1
942 mixture of mutant and WT cRNA, producing a left shift of -198 mV with 300 µM Ca^{2+} at the
943 inner membrane surface. This can be compared to a left shift of -120 mV with 0 Ca^{2+} (Fig.
944 3). Hence, the aberrant left shift in V_h induced by a 1:1 injection of mutant and WT
945 cRNA occurs in the presence and absence of intracellular Ca^{2+}.

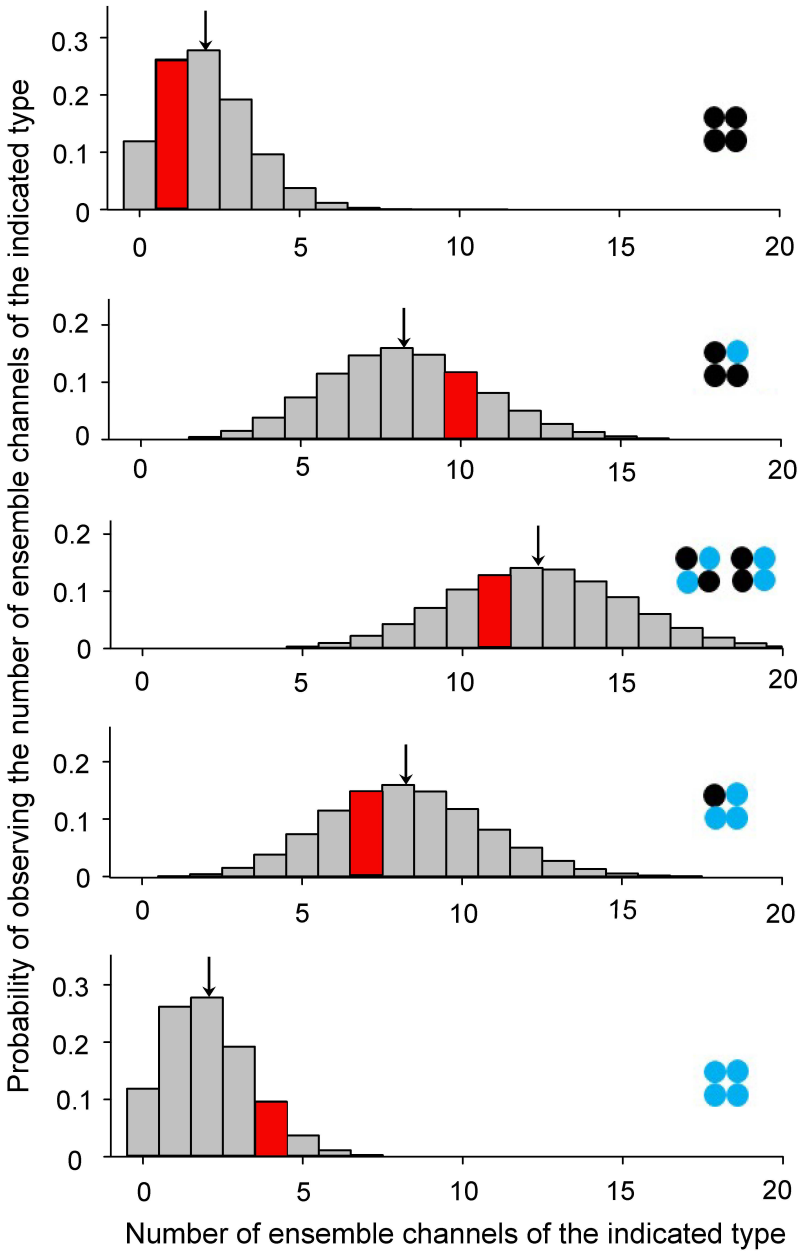

946 **Supplementary Fig. 4 The experimentally observed percentages of the five types of**
947 **assembled channels expressed following a 1:1 injection of G375R mutant and WT cRNA did**
948 **not differ significantly from the theoretical percentages in Fig. 1 calculated assuming**
949 **random assembly of mutant and WT subunits.** To examine if the experimentally observed
950 number of assembled channels of each type in Fig. 6 for the 33 assembled channels are
951 consistent with random assembly of subunits, we compared the experimental number of each
952 type to the expectations for random assembly. The expected number were determined by
953 simulating 106 groups of 33 assembled channels and binning the number of assembled
954 channels of each type for each group of 33 into five discrete probability distributions. The five
955 panels in this figure present the five discrete probability distributions of the expected number
956 of assembled channels of each type for a group of 33 channels. The channel type of each
957 distribution is indicated by subunit composition, where black circles are WT subunits and
957 blue circles are mutant

958 subunits. The topmost discrete probability distribution gives the mean probabilities based on
959 random assembly of subunits (Fig. 1) of observing the indicated number of WT channels in
960 a group of 33 assembled channels: 11.9% of the groups of 33 assembled channels would
961 have 0 WT assembled channels, 26.2% of the groups of 33 assembled channels
962 would have 1 WT assembled channel (red bar), 27.8% of the groups of 33 assembled
963 channels would have 2 WT assembled channels, and so forth. The arrow at 2.06 WT
964 channels indicates the mean number of predicted WT channels per group of 33 assembled
965 channels, determined from the discrete probability distribution. The mean number
966 can also be calculated directly from the percentages in Fig. 1: 6.25% of the
967 assembled channels are WT times 33 assembled channels equals a mean of 2.06
968 WT assembled channels for each group of 33. Discrete probability distributions for
969 each of the four other types of assembled channels in Fig. 1, are also presented and
970 are interpreted in a similar manner. For example, the discrete probability distribution for
971 channels with 1 mutant subunit and 3 WT subunits indicates that 7.34% of the groups
972 of 33 assembled channels would contain 5 channels of this type, 11.5% of the groups
973 of 33 channels would contain 6 channels of this type, and so forth.
974 Our experimental observations of the numbers of assembled channels of each type for
975 the experimental group of 33 assembled channels (Fig. 4D and 6A, B) are
976 indicated by the locations of the red histogram bars on the abscissa. The amplitude of
977 the red bars gives the probability of observing the indicated number of channels of
978 that type in the experimental group of 33 assembled channels. For example, the
979 probability, assuming random assembly of subunits, for our observation of 1
980 WT channel in the experimental group of 33 assembled channels was 0.262, and
981 the probabilities for our observations of 10, 11, 7, and 4 assembled channels for the
982 other indicated types of assembled channels in the experimental group of 33
983 assembled channels were 0.118, 0.128, 0.147, and 0.0961. All of these probabilities for
984 the observed numbers of assembled channels of each type were > 0.05 and none of the
985 observed numbers of assembled channel types fell within the 0.05 cumulative
986 probability of either the left or right tails of the discrete probability distributions,
987 indicating that the experimental observations for the number of the five types of
988 assembled channels were not significantly different[3] from the theoretical predictions
989 based on an assumption of random subunit assembly. A lack of significant difference
990 does not exclude that there may be underlying differences between experimental and
991 theoretical predictions, which could be revealed by larger sample sizes.
992
993 **References for the Supplementary Information**
994
995
996 1. Tao, X. & MacKinnon, R. Molecular structures of the human Slo1 K^+ channel in complex
997 with beta4. Elife 2019 Dec 9;8:e51409. doi: 10.7554/eLife.51409
998
999 2. Chen, X., Yan, J. & Aldrich, R. W. BK channel opening involves side-chain reorientation of
1000 multiple deep-pore residues. Proc. Nat. Acad. Sci. 111:E79-88 (2014).
1001
1002 3. D. Colquhoun, Lectures on Biostatistics (Clarendon Press, Oxford, 1971).